Journal of Statistical Physics (2021) 183:49
https://doi.org/10.1007/s10955-021-02774-6

Non-intersecting Brownian Bridges in the Flat-to-Flat Geometry

Jacek Grela[1] · **Satya N. Majumdar**[2] · **Grégory Schehr**[3]

Received: 4 March 2021 / Accepted: 11 May 2021 / Published online: 10 June 2021

Abstract
We study N vicious Brownian bridges propagating from an initial configuration $\{a_1 < a_2 < \ldots < a_N\}$ at time $t = 0$ to a final configuration $\{b_1 < b_2 < \ldots < b_N\}$ at time $t = t_f$, while staying non-intersecting for all $0 \leq t \leq t_f$. We first show that this problem can be mapped to a non-intersecting Dyson's Brownian bridges with Dyson index $\beta = 2$. For the latter we derive an exact effective Langevin equation that allows to generate very efficiently the vicious bridge configurations. In particular, for the flat-to-flat configuration in the large N limit, where $a_i = b_i = (i-1)/N$, for $i = 1, \ldots, N$, we use this effective Langevin equation to derive an exact Burgers' equation (in the inviscid limit) for the Green's function and solve this Burgers' equation for arbitrary time $0 \leq t \leq t_f$. At certain specific values of intermediate times t, such as $t = t_f/2$, $t = t_f/3$ and $t = t_f/4$ we obtain the average density of the flat-to-flat bridge explicitly. We also derive explicitly how the two edges of the average density evolve from time $t = 0$ to time $t = t_f$. Finally, we discuss connections to some well known problems, such as the Chern–Simons model, the related Stieltjes–Wigert orthogonal polynomials and the Borodin–Muttalib ensemble of determinantal point processes.

Keywords Brownian bridges · Nonintersecting brownian motions · Random matrices

Communicated by Pierpaolo Vivo.

✉ Grégory Schehr
gregory.schehr@u-psud.fr

Jacek Grela
jacekgrela@gmail.com

Satya N. Majumdar
majumdar@lptms.u-psud.fr

[1] Institute of Theoretical Physics, Jagiellonian University, 30-348 Cracow, Poland

[2] LPTMS, CNRS, Univ. Paris-Sud, Université Paris-Saclay, 91405 Orsay, France

[3] Sorbonne Université, Laboratoire de Physique Théorique et Hautes Energies, CNRS UMR 7589, 4 Place Jussieu, 75252 Paris Cedex 05, France

1 Introduction

The simplest way to generate a Brownian trajectory in one dimension is to evolve the position of a particle with time, starting say from $x(0) = 0$, via the stochastic Langevin equation

$$\frac{dx}{dt} = \sqrt{2D}\,\eta(t)\ , \tag{1}$$

where D is the diffusion constant and $\eta(t)$ is a Gaussian white noise with zero mean and two-time correlator $\langle \eta(t)\eta(t')\rangle = \delta(t-t')$. In many practical situations one needs to generate a constrained Brownian motion, e.g., a Brownian bridge that starts at $x(0) = a$ and ends at $x(t_f) = b$ after a fixed time t_f. Naively, one would generate all possible free Brownian configurations and retain, amongst them, only those that satisfy the bridge condition. Numerically, this is of course extremely inefficient. In the probability literature, such conditioned Brownian motions have been studied extensively pioneered by Doob [1,2], where one works out the transition probability of the effective Markov process that satisfies this constraint—known as the Doob transform. However, for numerical purposes, it is desirable to write explicitly an effective Langevin equation that generates constrained Brownian motions (such as the bridge) with the correct statistical weight [3,4]. It has been shown recently [5,6] how to construct explicitly such an effective Langevin equation for a class of constrained stochastic Markov processes in which the constraint manifests itself explicitly as an additional force in the Langevin equation. In the case of the Brownian bridge, this effective equation reads [5]

$$\frac{dx(t)}{dt} = \frac{b - x(t)}{t_f - t} + \sqrt{2D}\,\eta(t)\ , \tag{2}$$

where $\eta(t)$ is the same Gaussian white noise. Note that the force-term in (2) is time dependent and its presence ensures that the particle reaches b exactly at time t_f. The procedure used in [5] is rather general and has been used to derive the effective Langevin equation for several other constrained stochastic processes, such as an Ornstein–Uhlenbeck bridge, Brownian excursion, meander, etc [5]. This was done for the case of a single particle under constraints. It is then natural to wonder if one can develop a similar approach for many-body interacting Brownian particles.

A particularly simple model of interacting walkers is the so-called "vicious walkers" model introduced by de Gennes [7], followed by Fisher [8] and others [9–22]. There have been a lot of applications of this model both in statistical physics, for example in the context of fibrous polymers [7] or the melting and wetting transition in solids [8,9], all the way to combinatorics [23] and computer science [24]. Here one considers N Brownian motions starting at $a_1 < a_2 < \cdots < a_N$ and their positions $\{x_1(t), x_2(t), \cdots, x_N(t)\}$ at time t evolve via the free Langevin Eq. (1) except that they are constrained never to cross each other. In this model, for fixed N, there is thus just one parameter, namely the diffusion constant D, which is assumed to be the same for all the particles. Because of the non-intersection constraints, their positions at any time t remain ordered, i.e., $x_1(t) < x_2(t) < \cdots < x_N(t)$, provided they are ordered initially.

A natural practical question is: how to generate numerically a bridge configuration for such vicious Brownian motions that start at $a_1 < a_2 < \cdots < a_N$ at $t = 0$ and end at $b_1 < b_2 < \cdots < b_N$ at time $t = t_f$. Such vicious Brownian bridges (VBB) are known in the literature as "watermelons" (because they look like one) and they appear naturally in both physics and computer science. Finding an efficient algorithm to generate a watermelon configuration is a challenging problem [24]. A naive answer to this question would be to generate configurations of N free Brownian bridges, up to time t, and then retain only those

where the positions do not cross each other during the interval $[0, t_f]$. But this obviously is a rather wasteful algorithm.

In this paper, generalising the formalism of Ref. [5] to N non-intersecting Brownian motions, we provide an exact algorithm to generate a VBB. For reasons that will be clear later, we will henceforth denote the positions of the N particles in VBB by $\{\lambda_1(t) < \lambda_2(t) < \cdots < \lambda_N(t)\}$. We will proceed in two steps: (i) First we make an exact mapping between the VBB with diffusion constant $D = 1/(2N)$ and the so-called Dyson Brownian Bridge (DBB) with Dyson index $\beta = 2$ (for a precise definition of the DBB see Sect. 2). We show that under this mapping the positions of the N walkers in the VBB model, at any intermediate time $0 \le t \le t_f$, coincide in law with the positions of the N particles of DBB (with $\beta = 2$) at the same time t. By "coincide in law" one means that the joint distribution of the positions at any intermediate time are identical in both models. Therefore, if we can generate numerically the configurations of the DBB (with $\beta = 2$), this will automatically generate a configuration of the VBB model. (ii) Next we show that one can write an exact effective Langevin equation to generate the configurations of the DBB with $\beta = 2$. In particular, when the final positions are uniformly distributed over the interval [0, 1], obtained by choosing $b_i = (i-1)/N$, this effective Langevin equation becomes totally explicit. Thus (i) and (ii) together provide us with an exact algorithm to generate the configurations of the VBB.

In addition to providing a numerically efficient algorithm to generate a watermelon configuration, we show that our explicit Langevin equation, for the case when both the initial and the final configurations are uniformly distributed ("flat to flat"), i.e. $a_i = b_i = (i-1)/N$, with $i = 1, 2, \cdots, N$, can be successfully exploited analytically to compute certain observables in the large N limit, such as the average density $\rho^{(\lambda)}(\lambda; t) = \lim_{N\to\infty} \frac{1}{N} \langle \sum_{i=1}^{N} \delta(\lambda - \lambda_i(t)) \rangle$ of the walkers at any intermediate time in the interval $[0, t_f]$. In particular, we provide explicit formulae for $\rho^{(\lambda)}(\lambda; t)$ at $t = t_f/4$, $t = t_f/3$, $t = t_f/2$—note that the average density is symmetric around $t = t_f/2$ for the flat-to-flat case. Hence the density at t and $t_f - t$ are identical. We note that the previous result was known, by completely different methods, only for $t = t_f/2$. Indeed this particular case $t = t_f/2$ appeared in two apparently unrelated contexts, namely the Chern–Simons theory [25,26] and the theory of Stieltjes–Wigert orthogonal polynomials [27–30]. In fact, this problem also has some connections to the computation of the Harish-Chandra-Itzykson-Zuber (HCIZ) integral with flat initial and final configurations of the eigenvalues of two matrices A and B [31–33]. For other values of t, determining $\rho^{(\lambda)}(\lambda; t)$ explicitly is hard. However, one can show that $\rho^{(\lambda)}(\lambda; t)$ has a finite support $[\lambda_-(t), \lambda_+(t)]$ and we are able to compute explicitly how the support edges $\lambda_\pm(t)$ evolve with time [see Eq. (90)].

The organisation of the paper is best seen in Fig. 1. In Sect. 2 we provide (i) the mapping between the VBB and the DBB with $\beta = 2$ and (ii) derive the exact effective Langevin equations for the N-particle DBB for $\beta = 2$ where the final positions are equi-spaced (flat density). Next, in Sect. 3, we provide a derivation of the evolution equation of the Green's function and show that, in the large N limit, it reduces to the inviscid Burgers' equation, which can then be solved using the method of characteristics. In Sect. 4, we focus on the case where both the initial and the final density are flat and we compute explicitly the large N average density for three specific values of the time instants, namely $t = t_f/4, t_f/3$ and $t = t_f/2$, and these are detailed in Sect. 4.1–4.3 respectively. In Sect. 4.4, we derive explicitly the time evolution $\lambda_\pm(t)$ of the edges of the support of the average density $\rho(\lambda; t)$. We also provide in Sect. 4.5 a recursive derivation of the moments of the average density. In Sect. 5 we relate the flat-to-flat VBB to other models such as the Chern–Simons model and the theory of the biorthogonal Stieltjes–Wigert polynomials appearing in Muttalib-Borodin ensembles. Finally, we conclude in Sect. 6 with a summary and outlook.

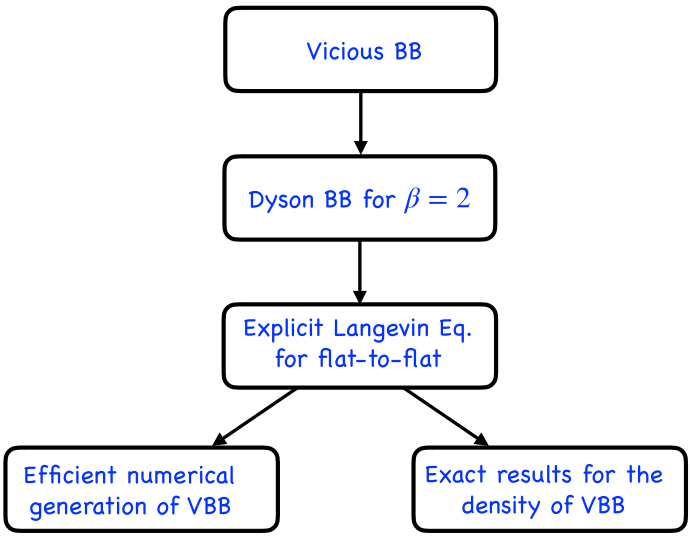

Fig. 1 Schematic organisation of the paper where BB stands for Brownian bridge and VBB stands for vicious Brownian bridge

2 The Mapping Between the VBB and DBB and an Effective Langevin Equation for the DBB

2.1 The Exact Equivalence Between the VBB and DBB with $\beta = 2$

We start with the vicious walkers bridge (VBB) starting at $t = 0$ from $\vec{a} = \{a_1, a_2, \cdots, a_N\}$ with $a_1 < a_2 < \cdots < a_N$, and ending at $t = t_f$ at $\vec{b} = \{b_1, b_2, \cdots, b_N\}$ with $b_1 < b_2 < \cdots < b_N$ (see Fig. 2). Let $\vec{\lambda}(t) = \{\lambda_1(t), \lambda_2(t), \cdots, \lambda_N(t)$ denote the positions of the N walkers in the VBB at an intermediate time t. Each of the λ_i's evolves locally in time via the Langevin equation

$$\frac{d\lambda_i}{dt} = \sqrt{2\,D}\,\eta_i(t)\ , \tag{3}$$

where η_i's are again Gaussian white noises with zero mean and correlator $\langle \eta_i(t)\eta_j(t')\rangle = \delta_{i,j}\delta(t-t')$. Here D is the diffusion constant that we assume to be the same for each walker. To compute the joint distribution $P_{\mathrm{VBB},D}(\vec{\lambda}, t|\vec{b}, \vec{a}, t_f)$ of these positions at time t, given the initial and final positions, we proceed as follows. Dividing the time interval $[0, t_f]$ into $[0, t]$ and $[t, t_f]$ with $0 \le t \le t_f$ and using the Markov property of the process, we get

$$P_{\mathrm{VBB},D}(\vec{\lambda}, t|\vec{b}, \vec{a}, t_f) = \frac{P_{\mathrm{VBM},D}(\vec{\lambda}, t|\vec{a}, 0)\; P_{\mathrm{VBM},D}(\vec{b}, t_f|\vec{\lambda}, t)}{P_{\mathrm{VBM},D}(\vec{b}, t_f|\vec{a}, 0)}\ , \tag{4}$$

where $P_{\mathrm{VBM},D}(\vec{\lambda}, t|\vec{a}, 0)$ denotes the propagator from time 0 to time t of the free vicious Brownian motion (VBM)—without the bridge constraint. This means the propagator for N non-intersecting Brownian motions starting from $\vec{a}$ at $t = 0$ to $\vec{\lambda}$ at time t. We then need to compute this propagator for VBM, as an intermediate step, to compute the joint distribution of the VBB via Eq. (4). We now show that this propagator $P_{\mathrm{VBM},D}(\vec{\lambda}, t|\vec{a}, 0)$ can be related to the propagator of the so-called Dyson Brownian motion (DBM) with $\beta = 2$.

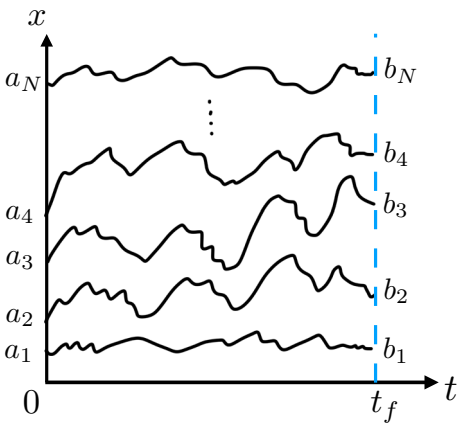

Fig. 2 Sketch of the trajectories of a VBB starting form $\vec{a}$ at time $t = 0$ and ending at $\vec{b}$ at time t_f

Let us first recall the definition of the DBM with Dyson index β. In DBM, one again considers N particles on a line, with positions $\lambda_i(t)$ with $i = 1, 2, \cdots, N$, that evolve via the stochastic equation

$$\frac{d\lambda_i(t)}{dt} = \frac{1}{N} \sum_{j(\neq i)=1}^{N} \frac{1}{\lambda_i(t) - \lambda_j(t)} + \sqrt{\frac{2}{\beta\, N}}\, \xi_i(t)\ , \tag{5}$$

where $\xi_i(t)$ are zero mean Gaussian white noises with correlations $\langle \xi_i(t)\xi_j(t')\rangle = \delta_{ij}\delta(t-t')$. The DBM, for fixed N, has only one parameter β, known as the Dyson's index. This model comes from random matrix theory (RMT) where one considers $N \times N$ random matrices (real symmetric, complex Hermitian or complex quaternionic) where the entries undergo independent Brownian motions as in Eq. (1). At each time t, if one diagonalises the matrix, one gets N real eigenvalues $\{\lambda_1(t) < \lambda_2(t) < \cdots < \lambda_N(t)\}$. Dyson, using second order perturbation theory, demonstrated [34] that the eigenvalues evolve via the stochastic equations (5). The parameter $\beta = 1, 2$ and 4 correspond to the real symmetric, complex Hermitian or complex quaternionic matrices. The force term on the right hand side of Eq. (5) comes from the effective pairwise repulsion between the eigenvalues. Even though originally only three quantized values of $\beta = 1, 2, 4$ were studied due to their relation with the symmetry classes of Gaussian matrices, it was later shown that there are actually matrix models which give rise to this Langevin Eq. (5) for arbitrary $\beta > 0$ [35]. The trajectories of the DBM, for arbitrary $\beta > 0$, can be easily generated numerically by evolving the positions of the walkers according to Eq. (5) starting from ordered initial positions $a_1 < a_2 < \cdots < a_N$. What is the connection between the two models: (i) VBM with parameter D and (ii) DBM with parameter β?

To see this connection, we first note that the propagator in the VBM with diffusion constant D satisfies the Fokker-Planck equation in the region $\lambda_1 \leq \lambda_2 \leq \cdots \leq \lambda_N$

$$\frac{\partial P_{\rm VBM}(\vec{\lambda}, t)}{\partial t} = D \sum_{i=1}^{N} \frac{\partial^2 P_{\rm VBM}(\vec{\lambda}, t)}{\partial \lambda_i^2}\ , \tag{6}$$

starting from the initial condition $P_{\rm VBM}(\vec{\lambda}, t = 0) = \delta(\vec{\lambda} - \vec{a})$. Note that, for simplicity of notations, we have omitted the explicit dependence of $P_{\rm VBM}(\vec{\lambda}, t)$ on $\vec{a}$ in Eq. (6). In addition,

$P_{\rm VBM}(\vec{\lambda}, t)$ satisfies the boundary conditions

$$P_{\rm VBM}(\lambda_i = \lambda_j, t) = 0 \quad \forall\, i \neq j \ . \tag{7}$$

These boundary conditions ensure the non-intersection constraint.

Now consider the DBM in Eq. (5). The associated Fokker-Planck equation in the region $\lambda_1 < \lambda_2 < \cdots < \lambda_N$ evolves as

$$\frac{\partial P_{\rm DBM}(\vec{\lambda}, t)}{\partial t} = \frac{1}{\beta N} \sum_{i=1}^{N} \frac{\partial^2 P_{\rm DBM}(\vec{\lambda}, t)}{\partial \lambda_i^2} - \sum_{i=1}^{N} \frac{\partial}{\partial \lambda_i} \left(E_i(\vec{\lambda}) P_{\rm DBM}(\vec{\lambda}, t) \right) \quad ;$$
$$\text{where} \quad E_i(\vec{\lambda}) = \frac{1}{N} \sum_{j(\neq i)=1}^{N} \frac{1}{\lambda_i - \lambda_j} \ , \tag{8}$$

with the initial condition $P_{\rm DBM}(\vec{\lambda}, t = 0) = \delta(\vec{\lambda} - \vec{a})$. The explicit repulsion term in (8) automatically ensures that the propagator $P_{\rm DBM}(\vec{\lambda}, t)$ vanishes whenever $\lambda_i = \lambda_j$ with $i \neq j$ as in Eq. (7). To relate this propagator to that of the VBM, we first make the transformation

$$P_{\rm DBM}(\vec{\lambda}, t) = \left(\frac{\Delta(\vec{\lambda})}{\Delta(\vec{a})} \right)^{\beta/2} W(\vec{\lambda}, t) \ , \tag{9}$$

where $\Delta(\vec{\lambda}) = \prod_{i<j}(\lambda_j - \lambda_i)$ and similarly $\Delta(\vec{a}) = \prod_{i<j}(a_j - a_i)$ are Vandermonde determinants. Upon substituting this form (9) in Eq. (8) and after long but straightforward algebra one finds [36] that $W(\vec{\lambda}, t)$ satisfies

$$\frac{\partial W(\vec{\lambda}, t)}{\partial t} = \frac{1}{\beta N} \sum_{i=1}^{N} \frac{\partial^2 W(\vec{\lambda}, t)}{\partial \lambda_i^2} - \frac{\beta - 2}{2N} \sum_{i=1}^{N} \sum_{1 \leq j \neq i \leq N} \frac{1}{(\lambda_i - \lambda_j)^2} W(\vec{\lambda}, t) \ . \tag{10}$$

For general β, $W(\vec{\lambda}, t)$ can be interpreted as the imaginary time propagator for the quantum Calogero-Sutherland model. Note that for $\beta = 2$ the second term on the right hand side (rhs) of Eq. (10) vanishes and $W(\vec{\lambda}, t)$ then satisfies the same equation as (6) with $D = 1/(2N)$, with the same boundary and initial conditions. Hence, for $\beta = 2$ and $D = 1/(2N)$, using Eq. (9), we get the identity

$$P_{{\rm DBM}, \beta=2}(\vec{\lambda}, t | \vec{a}, 0) = \frac{\Delta(\vec{\lambda})}{\Delta(\vec{a})} P_{{\rm VBM}, D=\frac{1}{2N}}(\vec{\lambda}, t | \vec{a}, 0) \ . \tag{11}$$

We now consider a Dyson Brownian bridge (DBB) where the positions of N particles in the DBM (5) starting at $\vec{a}$ at time $t = 0$ are further constrained to reach $\vec{b}$ at time $t = t_f$. As was done for the case of the VBB in (4), one can again use the Markov property of the DBM to write the joint distribution $P_{{\rm DBB}, D}(\vec{\lambda}, t | \vec{b}, \vec{a}, t_f)$ of these positions at time t, given the initial and final positions as

$$P_{{\rm DBB}, \beta}(\vec{\lambda}, t | \vec{b}, \vec{a}, t_f) = \frac{P_{{\rm DBM}, \beta}(\vec{\lambda}, t | \vec{a}, 0)\, P_{{\rm DBM}, \beta}(\vec{b}, t_f | \vec{\lambda}, t)}{P_{{\rm DBM}, \beta}(\vec{b}, t_f | \vec{a}, 0)} \ . \tag{12}$$

Setting $\beta = 2$ and $D = 1/(2N)$, and plugging the relation (11) in Eqs. (4) and (12), we see that the Vandermonde terms Δ's cancel out giving us the exact relation

$$P_{{\rm VBB}, D=\frac{1}{2N}}(\vec{\lambda}, t | \vec{b}, \vec{a}, t_f) = P_{{\rm DBB}, \beta=2}(\vec{\lambda}, t | \vec{b}, \vec{a}, t_f) \ . \tag{13}$$

Note that this relation is valid for any time $0 \leq t \leq t_f$. This implies that the positions of the N walkers at any intermediate time t have the same statistics in the two models. Statistically speaking, this means that

$$\{\lambda_1(t), \lambda_2(t), \cdots, \lambda_N(t)\}_{\text{VBB}, D=\frac{1}{2N}} \equiv \{\lambda_1(t), \lambda_2(t), \cdots, \lambda_N(t)\}_{\text{DBB}, \beta=2} \tag{14}$$

where the symbol "$\equiv$" indicates equivalence in law. This relation tells us that if we know how to generate numerically a configuration of the DBB with $\beta = 2$, then that configuration will also be a configuration of the VBB with $D = 1/(2N)$. Note that this choice of $D = 1/(2N)$ is not restrictive at all since one can always rescale time in the original Langevin equation (3) to set the diffusion constant to any prescribed value. Thus our mapping constitutes the first step towards building an algorithm to generate a VBB configuration. The second step is to generate explicitly a DBB configuration with $\beta = 2$. For this, we will generalize the method developed in Ref. [5] to write an effective Langevin equation to generate a DBB with $\beta = 2$. This is done in the next subsection.

2.2 Effective Langevin Equation for the DBB with $\beta = 2$

In this subsection, we generalize the method of Ref. [5] to the case of a DBB of N particles and arbitrary positive index $\beta > 0$. The positions of the particles $\vec{\lambda}(t)$ evolve via the Langevin equations (5), starting from the initial positions $\vec{a}$. The joint distribution of the particle positions at any time t is given in Eq. (12). For convenience, we denote the second term in the numerator as

$$P_{\text{DBM},\beta}(\vec{b}, t_f|\vec{\lambda}, t) = Q(\vec{\lambda}, t|\vec{b}, t_f)\ . \tag{15}$$

Note that the left hand side (lhs) is the "forward" propagator from $\vec{\lambda}$ at time t to $\vec{b}$ at time t_f, while the rhs is the same quantity but interpreted as the "backward" (i.e., time reversed) propagator from $\vec{b}$ at time t_f to $\vec{\lambda}$ at time t. For convenience, we rewrite the numerator in (12) in a shorthand notation as

$$\tilde{P}(\vec{\lambda}, t) = P_{\text{DBM},\beta}(\vec{\lambda}, t|\vec{a}, 0)\ Q(\vec{\lambda}, t|\vec{b}, t_f)\ . \tag{16}$$

The goal is to derive a Fokker-Planck (FP) equation for $\tilde{P}(\vec{\lambda}, t)$, knowing the FP equations for $P_{\text{DBM},\beta}$ and $Q(\vec{\lambda}, t|\vec{b}, t_f)$. Using further shortcut notations $P \equiv P_{\text{DBM},\beta}$ and $Q \equiv Q(\vec{\lambda}, t|\vec{b}, t_f)$, it is easy to see, given the Langevin Eq. (5), that P and Q satisfy respectively the forward and backward FP equations

$$\partial_t P = \tilde{D} \sum_{i=1}^{N} \partial_{\lambda_i}^2 P - \sum_{i=1}^{N} \partial_{\lambda_i} \left[E_i(\vec{\lambda})\ P \right], \tag{17}$$

$$-\partial_t Q = \tilde{D} \sum_{i=1}^{N} \partial_{\lambda_i}^2 Q + \sum_{i=1}^{N} E_i(\vec{\lambda})\ \partial_{\lambda_i} Q, \tag{18}$$

where

$$\tilde{D} = \frac{1}{\beta N} \quad , \quad E_i(\vec{\lambda}) = \frac{1}{N} \sum_{j(\neq i)=1}^{N} \frac{1}{\lambda_i - \lambda_j}\ . \tag{19}$$

Note that in the equation for Q (18) on the lhs the time derivative has a negative sign. This is because the time is going backward. Since $\tilde{P} = P\,Q$, one gets

$$\partial_t \tilde{P} = Q\,\partial_t P + P\,\partial_t Q = \tilde{D}\sum_i \left[Q\,\partial^2_{\lambda_i} P - P\partial^2_{\lambda_i} Q\right] - \sum_i \left[Q\,\partial_{\lambda_i}\left(E_i(\vec{\lambda})\,P\right) + P\,E_i(\vec{\lambda})\,\partial_{\lambda_i} Q\right]. \tag{20}$$

We next use the following two identities

$$Q\partial^2_{\lambda_i} P - P\partial^2_{\lambda_i} Q = \partial^2_{\lambda_i}\tilde{P} - 2\partial_{\lambda_i}\left(\tilde{P}\,\partial_{\lambda_i}\log Q\right)\,, \tag{21}$$

$$Q\partial_{\lambda_i}\left(E_i(\vec{\lambda})\,P\right) + P\,E_i(\vec{\lambda})\,\partial_{\lambda_i} Q = \partial_{\lambda_i}\left(E_i(\vec{\lambda})\,\tilde{P}\right)\,, \tag{22}$$

to simplify the rhs of Eq. (20) and obtain a compact FP equation for $\tilde{P}$

$$\partial_t \tilde{P} = \tilde{D}\sum_i \partial^2_{\lambda_i}\tilde{P} - \sum_i \partial_{\lambda_i}\left[\left(E_i(\vec{\lambda}) + 2\,\tilde{D}\,\partial_{\lambda_i}\log Q\right)\tilde{P}\right]\,. \tag{23}$$

This FP equation corresponds exactly to an effective Langevin equation

$$\frac{d\,\lambda_i(t)}{dt} = E_i(\vec{\lambda}) + 2\,\tilde{D}\,\frac{\partial \ln Q}{\partial \lambda_i} + \sqrt{2\,\tilde{D}}\,\xi_i(t)\,, \tag{24}$$

where $\xi_i(t)$ is a Gaussian white noise with zero mean and correlator $\langle \xi_i(t)\xi_j(t')\rangle = \delta_{ij}\delta(t-t')$. Using the expressions for $\tilde{D}$ and E_i in Eq. (19), we finally get the effective Langevin equation of the DBB with arbitrary $\beta > 0$ as

$$\frac{d\,\lambda_i(t)}{dt} = \frac{1}{N}\sum_{j\neq i}\frac{1}{\lambda_i - \lambda_j} + \frac{2}{\beta N}\,\frac{\partial \ln Q}{\partial \lambda_i} + \sqrt{\frac{2}{\beta N}}\,\xi_i(t)\,. \tag{25}$$

Note that in this equation the second term represents the effective force due to the bridge constraint. Of course, one needs to know the backward propagator Q for the free DBM in order to compute this effective force term explicitly. For a general β, this is very hard. However, for $\beta = 2$, using the connection with the VBM, one can make progress. Indeed, in this case, using the relation (11), we get

$$Q(\vec{\lambda}, t|\vec{b}, t_f) = P_{\mathrm{DBM},\beta=2}(\vec{b}, t_f|\vec{\lambda}, t) = \frac{\Delta(\vec{b})}{\Delta(\vec{\lambda})}\,P_{\mathrm{VBM},D=\frac{1}{2N}}(\vec{b}, t_f|\vec{\lambda}, t)\,. \tag{26}$$

It turns out that the propagator for the VBM can be computed explicitly using the Karlin-McGregor formula [37]

$$P_{\mathrm{VBM},D}(\vec{b}, t_f|\vec{\lambda}, t) = \det_{1\le i,j\le N}\left[\frac{e^{-\frac{(b_i-\lambda_j)^2}{4\,D\,(t_f-t)}}}{\sqrt{4\pi\,D\,(t_f-t)}}\right]\,. \tag{27}$$

In general, it is not easy to evaluate this $N \times N$ determinant explicitly for arbitrary b_i's. However, for the special case where the final positions are equispaced (corresponding to a flat density over the interval $\lambda \in [0, 1]$)

$$b_i = \frac{i-1}{N}\,,\ i = 1, 2, \cdots, N\,, \tag{28}$$

this determinant can be explicitly evaluated as follows. Expanding the determinant in (27) we get

$$\det_{1\le i,j\le N}\left(\frac{e^{-\frac{(b_i-\lambda_j)^2}{4D(t_f-t)}}}{\sqrt{4\pi D(t_f-t)}}\right)=\frac{e^{-\frac{1}{4D(t_f-t)}\sum_j\lambda_j^2}e^{-\frac{1}{4D(t_f-t)}\sum_j b_j^2}}{\left[4\pi D(t_f-t)\right]^{N/2}}\det_{1\le i,j\le N}\left(e^{\frac{b_i\lambda_j}{2D(t_f-t)}}\right) \quad (29)$$

For the flat final condition (28) the determinant in (29) can be further simplified

$$\det_{1\le i,j\le N}\left(e^{\frac{b_i\lambda_j}{2D(t_f-t)}}\right)=\det_{1\le i,j\le N}\left(e^{\frac{(i-1)\lambda_j}{2DN(t_f-t)}}\right)=\prod_{i<j}\left(e^{\frac{\lambda_j}{2DN(t_f-t)}}-e^{\frac{\lambda_i}{2DN(t_f-t)}}\right), \quad (30)$$

where we have used the fact that $\det_{1\le i,j\le N} X_j^{i-1}=\prod_{i<j}(X_j-X_i)$. This gives

$$P_{\mathrm{VBM},D}(\vec{b},t_f|\vec{\lambda},t)\propto e^{-\frac{1}{4D(t_f-t)}\sum_{i=1}^N\lambda_i^2}\prod_{i<j}\left(e^{\frac{\lambda_j}{2DN(t_f-t)}}-e^{\frac{\lambda_i}{2DN(t_f-t)}}\right), \quad (31)$$

where the proportionality constant (omitted here) is independent of λ and does not play any role (as we will see shortly). Inserting this result in Eq. (26), and taking logarithm and using $D=1/(\beta N)=1/(2N)$ for $\beta=2$, gives

$$\ln Q=-\frac{N}{2(t_f-t)}\sum_{i=1}^N\lambda_i^2-\sum_{i<j}\ln(\lambda_j-\lambda_i)+\sum_{i<j}\ln\left(e^{\frac{\lambda_j}{t_f-t}}-e^{\frac{\lambda_i}{t_f-t}}\right)+A, \quad (32)$$

where A is a constant which is independent of $\vec{\lambda}$. Taking derivative of (32) with respect to λ_i and inserting in (25) we get an explicit Langevin equation

$$\frac{d\lambda_i}{dt}=-\frac{\lambda_i}{t_f-t}+\frac{1}{N(t_f-t)}\sum_{j(\neq i)}\frac{e^{\frac{\lambda_i}{t_f-t}}}{e^{\frac{\lambda_i}{t_f-t}}-e^{\frac{\lambda_j}{t_f-t}}}+\frac{1}{\sqrt{N}}\xi_i(t). \quad (33)$$

This equation starts from any arbitrary initial condition $\vec{a}$. It does generate the trajectories of the DBB with $\beta=2$ (and hence of the VBB with $D=1/(2N)$) where the final positions correspond to a flat density in Eq. (28). This completes our derivation of the Langevin equation for the VBB. Numerically it is easy to generate the trajectories of VBB using this equation. Examples of such trajectories are shown in Figs. 4, 5 and 7.

By examining the rhs of Eq. (33), it is natural to make the following change of variables

$$\begin{cases} x_i=e^{\frac{\lambda_i}{t_f-t}}, \\ \theta=\frac{t}{t_f-t}, \end{cases} \quad (34)$$

or equivalently

$$\begin{cases} \lambda_i=\frac{t_f}{1+\theta}\log x_i, \\ t=t_f\frac{\theta}{1+\theta}, \end{cases} \quad (35)$$

where the new space– and time–like variables become positive $x_i\in(0,\infty)$ and $\theta\in(0,\infty)$. Since $\theta=t/(t_f-t)$, the initial time $t=0$ is mapped to $\theta=0$ while the final time $t=t_f$

corresponds to $\theta \to \infty$. The Langevin equations (33) in terms of these new coordinates read (after some straightforward algebra)

$$\frac{dx_i}{d\theta} = \frac{1}{Nt_f} \sum_{j(\neq i)} \frac{x_i^2}{x_i - x_j} + \frac{1+\theta}{t_f} x_i \, \tilde{\xi}_i(\theta) \, , \tag{36}$$

where $\tilde{\xi}_i(\theta)$ is a Gaussian white noise with zero mean and correlator $\langle \tilde{\xi}_i(\theta) \tilde{\xi}_j(\theta') \rangle = \delta_{ij} \delta(\theta - \theta')$. Note that the drift term in this transformed Langevin Eq. (36) does not contain explicit θ-dependence, unlike the original Eq. (33) where the drift term depends on t explicitly. In addition, the noise term in (36) is multiplicative and we will interpret it in the Ito sense.

3 Average Particle Sensity via Burgers' Equation

In the previous section, we have shown how to generate numerically the configuration of a VBB, by generating a configuration of DBB with $\beta = 2$ via the explicit Langevin equation (33) for the case of a flat final density at $t = t_f$. In this section, we show that this effective Langevin equation is useful not just to generate a configuration numerically, but also to compute some physical observables, such as the density of the particles at an intermediate time $0 \leq t \leq t_f$.

3.1 Derivation of the Burgers' Equation

In this section we first discuss densities in both spaces (λ, t) [see Eq. (33)] and (x, θ) [see Eq. (36)] and a functional relation between them. We then introduce the Green's function as an intermediate tool to compute the average densities. To derive an evolution equation for the Green's function, it turns out to be convenient first to write an evolution equation for an object, analog of a characteristic polynomial. Using a Cole-Hopf relation between the characteristic polynomial and the Green's function, we can then derive an equation for the Green's function. It turns out that in the large N limit this evolution equation for the Green's function simplifies a lot allowing us to obtain certain explicit results.

We consider the positions $\vec{\lambda}(t)$ evolving via the Langevin Eq. (33) and define the density at time t

$$\rho_N^{(\lambda)}(\lambda; t) = \frac{1}{N} \left\langle \sum_{i=1}^{N} \delta(\lambda - \lambda_i(t)) \right\rangle \, , \tag{37}$$

where $\langle \cdots \rangle$ denotes an average over the random variables $\vec{\lambda}(t)$ in (33) and the superscript (λ) refers to the density in the λ-space. From now on, we consider all quantities with a subscript N as exact for any N whereas the corresponding asymptotic quantities lack the subscript $\rho^{(\lambda)} = \lim_{N \to \infty} \rho_N^{(\lambda)}$. Following the space-time transformation (35), the density in (x, θ) variables reads

$$\rho_N^{(x)}(x; \theta) = \frac{1}{N} \left\langle \sum_{i=1}^{N} \delta\left(x - x_i(\theta)\right) \right\rangle \, . \tag{38}$$

Since the transformation (35) is bijective, the relation between the two densities is straightforward

$$\rho_N^{(\lambda)}(\lambda;t) = \frac{e^{\frac{\lambda}{t_f-t}}}{t_f-t}\rho_N^{(x)}\left(x = e^{\frac{\lambda}{t_f-t}}; \theta = \frac{t}{t_f-t}\right). \tag{39}$$

One way of obtaining $\rho_N^{(x)}$ is by considering an associated Green's function (or resolvent)

$$G_N^{(x)}(y;\theta) = \frac{e^y}{Nt_f}\left\langle \sum_{i=1}^{N} \frac{1}{e^y - x_i(\theta)} \right\rangle , \tag{40}$$

which is defined on the whole complex y-plane with exception of the positions $e^y = x_i$. In our case, it is a real axis half–line $e^y > 0$ since $x_i > 0$. Knowing the Green's function, one can extract the average density using the Sochocki–Plemelj formula

$$\rho_N^{(x)} = \frac{t_f}{\pi} \lim_{\epsilon\to 0_+} \mathrm{Im}\left[\frac{1}{y} G_N^{(x)}(\ln y;\theta)\right]_{y=x-i\epsilon} , \tag{41}$$

where $\mathrm{Im}(z)$ denotes the imaginary part of z. Because we have already introduced the variables (x,θ) to ease the calculations, we do not define the Green's function corresponding to the (λ,t) space and only use relation (39) when needed.

Our goal next is to write an evolution equation for the Green's function $G_N^{(x)}(y;\theta)$. This however turns out to be hard for finite N. To make progress, we instead introduce the *characteristic polynomial*

$$\Omega_N(y;\theta) = \left\langle \prod_{i=1}^{N} \left(e^y - x_i(\theta)\right) \right\rangle , \tag{42}$$

where again we choose the usual argument to be in an exponential form e^y for convenience. It turns out that, starting from the Langevin Eq. (36), one can derive an exact evolution equation for $\Omega_N(y;\theta)$ for any finite N. The derivation is detailed in Appendix A. This equation reads

$$\partial_\theta \Omega_N = \frac{N-1}{2t_f}\Omega_N + \frac{1}{2Nt_f}\left(\partial_y\Omega_N - \partial_{yy}\Omega_N\right) . \tag{43}$$

Let us remark that the prefactor of the second derivative in the rhs is negative, i.e., corresponding to a negative diffusion constant $-1/(2Nt_f)$. We next define the logarithmic derivative

$$g_N(y;\theta) = \frac{1}{Nt_f}\partial_y \log\Omega_N(y;\theta) = \frac{1}{Nt_f}\partial_y \ln\left\langle \prod_{i=1}^{N}\left(e^y - x_i(\theta)\right)\right\rangle . \tag{44}$$

The evolution Eq. (43) in terms of $g_N(y;\theta)$ reads

$$\partial_\theta g_N = \frac{1}{2Nt_f}\left(\partial_y g_N - \partial_{yy} g_N\right) - g_N\partial_y g_N , \tag{45}$$

where we used the two identities $\partial_y\Omega_N = Nt_f g_N\Omega_N$ and $\partial_{yy}\Omega_N = Nt_f\Omega_N\partial_y g_N + (Nt_f g_N)^2\Omega_N$.

How do we relate the function $g_N(y;\theta)$ in Eq. (44) and the Green's function $G_N^{(x)}(y;\theta)$ defined in Eq. (40)? For any finite N these two functions are a priori different. Indeed,

$G_N^{(x)}(y;\theta)$ in Eq. (40) can be expressed as

$$G_N^{(x)}(y;\theta) = \frac{1}{N\,t_f}\partial_y \left\langle \ln \prod_{i=1}^{N} \left(e^y - x_i(\theta)\right) \right\rangle . \tag{46}$$

Comparing this expression to that of $g_N(y;\theta)$ in (44), we see that while in Eq. (44) the average $\langle \cdots \rangle$ is inside the argument of the logarithm, it is outside the logarithm in Eq. (46). However, typically in the limit of large N, the random variable inside the logarithm is highly peaked and the two averages coincide in that limit—this is known as the "self-averaging property". If the self-averaging property holds (which we will assume here), we then have

$$\lim_{N\to\infty} g_N(y;\theta) = \lim_{N\to\infty} G_N^{(x)}(y;\theta) = G^{(x)}(y;\theta) . \tag{47}$$

Taking this large N limit in Eq. (45), the first term in the rhs drops out and, using (47), we arrive at a very simple equation for the Green's function

$$\partial_\theta G^{(x)} + G^{(x)}\partial_y G^{(x)} = 0 . \tag{48}$$

Since θ is a time-like variable, this equation has to be solved subject to the initial condition

$$G^{(x)}(y,0) = G_0^{(x)}(y) , \tag{49}$$

where $G_0^{(x)}(y)$ depends on the choice of the initial positions $\vec{a}$. This is the well known Burgers' equation in fluid dynamics (in the inviscid limit) but in the complex y-plane, i.e., a first–order PDE with a non–linear term.

Note that the Burgers' Eq. (48) that we derived here is in the (x,θ) coordinates and is already tailored for the bridge configuration because both coordinates (x,θ) as defined in Eq. 35 already contains the information about the final time t_f and the final flat configuration. In fact, we recall that this Burgers' equation has been derived starting from the effective Langevin Eq. (36), which holds only for the bridge configuration, with a flat final density. On the other hand, for Dyson Brownian motion evolving via Eq. (5) one can define a similar Green's function

$$G_{\rm DBM}(z;t) = \frac{1}{N}\sum_{i=1}^{N} \frac{1}{z-\lambda_i(t)} . \tag{50}$$

It is then easy to show that, in the large N limit, this Green's function also satisfies the inviscid Burgers' equation [38–41]

$$\partial_t G_{\rm DBM}(z;t) + G_{\rm DBM}(z;t)\ \partial_z G_{\rm DBM}(z;t) = 0 , \tag{51}$$

starting from some initial configuration $G_{\rm DBM}(z;0)$. However, this Green's function does not hold for the bridge since it has no information on the future, in particular on the condition at $t = t_f$. Thus, this well known canonical Burgers' equation has nothing to do with the Burgers' equation for the vicious bridge (48) that we derived above. Let us emphasize once more that a crucial ingredient leading to the derivation of this Burgers' equation for the bridge is the use of the effective Langevin Eq. (33) that automatically took the bridge constraint into account. Furthermore, this bridge Burgers' equation (48) holds in the transformed coordinates (x,θ) and not in the original coordinates (λ,t).

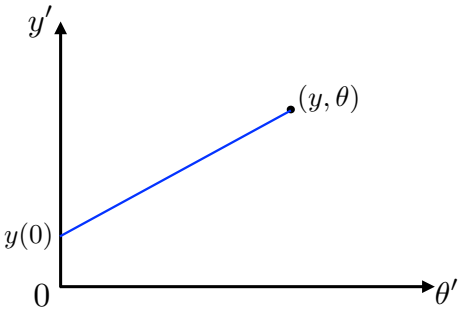

Fig. 3 Illustration of the characteristic (54) in the (y', θ') plane

3.2 Solution of the Burgers' Equation

The Burgers' Eq. (48) can be solved by the standard method of characteristics. Consider the (y', θ') plane with (y, θ) being one particular point on this plane. We consider a curve $y(\theta')$ in this plane that passes though the point (y, θ) at time $\theta' = \theta$ (see Fig. 3). We choose this curve such that $G^{(x)}(y(\theta'); \theta')$ is a constant along this curve. Therefore

$$\frac{d}{d\theta'} G^{(x)}(y(\theta'); \theta') = \frac{\partial G^{(x)}}{\partial \theta'} + \frac{\partial G^{(x)}}{\partial y} \frac{dy(\theta')}{d\theta'} . \tag{52}$$

Since $G^{(x)}$ is chosen to be a constant along this curve $y(\theta')$, this total derivative (52) is zero. By comparing the rhs of (52) with Eq. (48), we see that curve $y(\theta')$ (called the "characteristics") must satisfy the equation of motion

$$\frac{dy(\theta')}{d\theta'} = G^{(x)}(y; \theta) . \tag{53}$$

This equation is trivial to solve since $G^{(x)}(y; \theta)$ is a constant along the curve and we get a linear characteristic

$$y(\theta') = y(0) + \theta' \, G^{(x)}(y; \theta) . \tag{54}$$

Along this characteristics we then have

$$G^{(x)}(y, \theta) = G^{(x)}(y(\theta'), \theta') , \ \forall \, 0 \le \theta' \le \theta . \tag{55}$$

Setting $\theta' = 0$ in Eq. (55) we get

$$G^{(x)}(y, \theta) = G^{(x)}(y(0), 0) = G_0^{(x)}(y(0)) , \tag{56}$$

where $G_0^{(x)}$ is the initial Green's function (49). Furthermore, setting $\theta' = \theta$ in Eq. (54) and using $y(\theta) = y$, we can determine $y(0)$ in terms of the final value

$$y(0) = y - \theta \, G^{(x)}(y; \theta) . \tag{57}$$

Finally substituting this expression for $y(0)$ in Eq. (56) we get an exact self-consistent equation for $G^{(x)}(y; \theta)$

$$G^{(x)}(y, \theta) = G_0^{(x)}(y - \theta \, G^{(x)}(y; \theta)) \tag{58}$$

where $G_0^{(x)}(\xi)$ is a known function, set by the initial condition. Note that the solution is parametric in the following sense. We can rewrite Eq. (58) in the following way

$$G^{(x)}(y,\theta) = G_0^{(x)}(\xi) \quad \text{where} \quad \xi = y(0) = y - \theta G^{(x)}(y,\theta)\ . \tag{59}$$

The second equation gives

$$y = \xi + \theta\, G^{(x)}(y,\theta) = \xi + \theta\, G_0^{(x)}(\xi)\ , \tag{60}$$

where in the last equality we have used the first equality in Eq. (59). Thus, given y and θ, we have to first solve for ξ from Eq. (60) and then substitute this value of ξ to evaluate $G_0^{(x)}(\xi)$ and then (59) gives us $G^{(x)}(y,\theta)$. This is the parametric recipe to solve for the Green's function $G^{(x)}(y,\theta)$. The function $G_0^{(x)}(\xi)$ that corresponds to the initial Green's function plays a central role in the solution. For our problem, this is given by

$$G_0^{(x)}(\xi) = \frac{e^{\xi}}{t_f} \lim_{N\to\infty} \frac{1}{N} \sum_{i=1}^{N} \frac{1}{e^{\xi} - x_i^{(0)}}. \tag{61}$$

The initial values $x_i^{(0)}$ and $\lambda_i^{(0)} = a_i$ are related through the transformation (35) as $x_i^{(0)} = e^{a_i/t_f}$. In the following section we consider a flat-to-flat VBB where both the starting points and end points have the same flat density, i.e., $a_i = b_i = (i-1)/N$.

4 Particle Density for a Flat-to-Flat VBB

In this section, we compute the average density both in the (λ, t)-coordinates (37) and equivalently in the (x,θ) coordinates (38). We consider the $\beta = 2$ DBB, that starts and ends at the flat configuration $a_i = b_i = (i-1)/N$. At $t = 0$, and in the large N limit, the initial condition thus corresponds to a uniform flat density in the λ-variable

$$\rho^{(\lambda)}(\lambda; 0) = 1 \quad \text{for} \quad 0 \le \lambda \le 1\ , \tag{62}$$

and the density vanishes outside the support $\lambda \in [0,1]$. By virtue of the transformation (34) we have, at $t = 0$, $x_i = e^{\lambda_i/t_f}$. Consequently, the density in the x-variable at $\theta = 0$ (corresponding to $t = 0$) reads

$$\rho^{(x)}(x; 0) = \frac{t_f}{x} \quad \text{for} \quad 1 \le x \le e^{1/t_f}\ , \tag{63}$$

and the density vanishes outside the support $x \in [1, e^{1/t_f}]$. It is then easily to check that the density is normalized in the x-variables, i.e., $\int_1^{e^{1/t_f}} \rho^{(x)}(x;0)\, dx = 1$.

In the Sect. 1, we show that the equation for the Green's function (58) and (61) in the $(\vec{x},\theta)$ coordinates can be written in a compact form. It turns out that it allows an explicit solution only for three values of $\theta = 1, 2$ and 3, corresponding respectively to $t = t_f/2$, $t = 2t_f/3$ and $t = 3t_f/4$. In Sect 2, we first derive explicitly the average density for $\theta = 1$. Subsequently, in Sect 3, the explicit results for the average density are derived respectively for $t = 2t_f/3$ and $t = 3t_f/4$ (and thus equivalently for $t = t_f/3$ and $t = t_f/4$ thanks to the symmetry around $t = t_f/2$). In Sect. 4, we compute explicitly how the edges of the support of the average density $[\lambda_-(t), \lambda_+(t)]$ evolve with time t for all $0 \le t \le t_f$. Finally, in Sect. 5, we provide some exact results for the moments of the average density for any $0 \le t \le t_f$.

4.1 Solution in Terms of e-Green's Function $H = e^{-G^{(x)}}$

Formula (58) is the solution to Burgers' equation (48) depending only on the initial function (61). In the flat case $a_i = \frac{1}{N}(i-1)$ it is found by the Euler-Maclaurin formula that

$$G^{(x)}(y;0) = G_0^{(x)}(y) = \lim_{N\to\infty} \frac{e^y}{Nt_f} \sum_{i=1}^{N} \frac{1}{e^y - e^{\frac{i-1}{Nt_f}}} = \frac{e^y}{t_f} \int_0^1 du \frac{1}{e^y - e^{u/t_f}} = \ln\left(\frac{1-e^y}{1-e^{y-1/t_f}}\right), \tag{64}$$

which is defined everywhere in the complex y-plane, with a cut on the real y-axis over the interval $y \in (0, 1/t_f)$. We plug the initial function (64) into the solution (58) and obtain

$$e^{G^{(x)}}\left(1 - e^{y-\theta G^{(x)} - 1/t_f}\right) = 1 - e^{y-\theta G^{(x)}}. \tag{65}$$

This form (65) leads us naturally to define an exponentiated Green's (or e-Green's) function

$$H(w;\theta) = e^{-G^{(x)}(y;\theta)} \quad , \quad \text{where} \quad w = e^y \quad \text{and} \quad T = e^{-1/t_f}. \tag{66}$$

This then gives us a compact transcendental equation for $H(w;\theta)$

$$H^\theta = \frac{1}{w}\frac{1-H}{T-H}, \tag{67}$$

where we recall that $\theta = t/(t_f - t)$.

Although for general time θ, the e-Green's function H cannot be found by analytic methods, we will still extract useful information out of it. In particular, the Sochocki–Plemejl formula giving the particle density $\rho^{(x)}$ in terms of the e-Green's function $\rho^{(x)}(x;\theta) = -\frac{t_f}{\pi}\lim_{\epsilon\to 0_+} \mathrm{Im}\left[\frac{1}{w}\ln H(w;\theta)\right]_{w=x-i\epsilon}$ is found as (see Appendix B)

$$\rho^{(x)}(x;\theta) = -\frac{t_f}{\pi x}\lim_{\epsilon\to 0_+} \arg H(x - i\epsilon;\theta). \tag{68}$$

The scheme for obtaining particles densities in both (λ, t) and (x, θ) variables is the following—compute the H by solving Eq. (67), use Sochocki–Plemejl formula (68) to find $\rho^{(x)}$ and lastly compute $\rho^{(\lambda)}$ by formula (39).

4.2 Particle Density for $t = t_f/2$ ($\theta = 1$)

Since both initial and final positions are equal, the instant $t = t_f/2$ is special due to the symmetry $t \to t_f - t$ which makes the calculation of the density easier. When $t = t_f/2$, which corresponds to $\theta = t/(t_f - t) = 1$, Eq. (67) reduces to a quadratic equation

$$wH^2 - wTH - H + 1 = 0,$$

which has two explicit solutions $H_\pm(w;\theta=1) = \frac{1}{2w}\left(1 + wT \pm T\sqrt{-r_1(w)}\right)$ where

$$r_1(w) = (w_+^{(1)} - w)(w - w_-^{(1)}) \quad , \quad \text{with} \quad w_\pm^{(1)} = \frac{2 - T \pm 2\sqrt{1-T}}{T^2}. \tag{69}$$

To choose the correct root, we proceed as follows. From Eq. (40), we see that, as $y \to \infty$, $G^{(x)}(y;\theta=1) \to 1/t_f$. Consequently $H(w = e^y;\theta) = e^{-G^{(x)}(y;\theta)} \to e^{-1/t_f} = T$. Hence,

as $w \to \infty$, we must have $H(w;\theta) \to T$. Therefore we choose $H(w;\theta=1) = H_+(w;\theta=1)$.

To use the formula for the density in (68), we set $w = x - i\epsilon$ and expand around $\epsilon = 0$, yielding

$$H_+ = C_1 + iC_2\epsilon + \mathcal{O}(\epsilon^2), \tag{70}$$

where $C_1 = H_+(x) = \frac{1+xT+T\sqrt{-r_1(x)}}{2x}$, $C_2 = -H'_+(x) = \frac{1-2x+Tx+T\sqrt{-r_1(x)}}{2x^2T\sqrt{-r_1(x)}}$. We consider two cases:

- For $r_1(x) < 0$ or when $x \notin (w_-^{(1)}, w_+^{(1)})$, both C_1 and C_2 are real functions and so the following result holds

$$\lim_{\epsilon\to 0_+} \arg H(x - i\epsilon;\theta) = \lim_{\epsilon\to 0_+} \arctan\left[\frac{C_2}{C_1}\epsilon\right] = 0. \tag{71}$$

  Consequently, the density vanishes for arguments outside of the interval $(w_-^{(1)}, w_+^{(1)})$.
- For $r_1(x) > 0$ or when $x \in (w_-^{(1)}, w_+^{(1)})$, the square–root term $\sqrt{-r_1(x)}$ becomes imaginary $\sqrt{-r_1(x)} = \sigma i\sqrt{r_1(x)}$ where $\sigma = \pm 1$ is the square–root branch parameter and will be fixed later. Now the expansion (70) is no longer properly ordered into real and imaginary parts. Instead, we have $C_1 = \frac{1+xT}{2x} + i\sigma T\frac{\sqrt{r_1(x)}}{2x}$, $C_2 = \frac{1}{2x^2} - \sigma i\frac{1-2x+Tx}{2x^2T\sqrt{r_1(x)}}$ which renders $H_+ = C'_1 + iC'_2 + \mathcal{O}(\epsilon^2)$ with $C'_1 = \frac{1+xT}{2x} + \sigma\epsilon\frac{1-2x+Tx}{2x^2T\sqrt{r_1(x)}}$, $C'_2 = \sigma T\frac{\sqrt{r_1(x)}}{2x} + \frac{\epsilon}{2x^2}$. This rearrangement makes the argument of H_+ non–zero inside the interval $(w_-^{(1)}, w_+^{(1)})$:

$$\lim_{\epsilon\to 0_+} \arg H_+ = \lim_{\epsilon\to 0_+} \arctan\left[\frac{C'_2}{C'_1}\right] = \arctan\left[\frac{\sigma T\sqrt{r_1(x)}}{1+xT}\right]. \tag{72}$$

  We fix $\sigma = -1$ by demanding that the argument (and the overall density) be positive.

We combine Eqs. (71) with (72) resulting in a particle density bounded to a finite interval:

$$\rho^{(x)}(x;\theta=1) = \begin{cases} 0 & , \quad x \notin (w_-^{(1)}, w_+^{(1)}) \\ \frac{t_f}{\pi x}\arctan\left[\frac{T\sqrt{r_1(x)}}{1+xT}\right] & , \quad x \in (w_-^{(1)}, w_+^{(1)}) \end{cases}. \tag{73}$$

The density is continuous as the function vanishes at the boundaries $r_1(w_\pm^{(1)}) = 0$ and so does $\arctan(0) = 0$. The density in λ variable is in turn given by Eq. (39) as:

$$\rho^{(\lambda)}\left(\lambda; t = t_f/2\right) = \begin{cases} 0 & , \quad \lambda \notin \left(\lambda_-^{(1)}, \lambda_+^{(1)}\right) \\ \frac{2}{\pi}\arctan\left(T\frac{\sqrt{r_1\left(e^{2\lambda/t_f}\right)}}{1+Te^{2\lambda/t_f}}\right) & , \quad \lambda \in \left(\lambda_-^{(1)}, \lambda_+^{(1)}\right) \end{cases}, \tag{74}$$

where the endpoints are given by $\lambda_\pm^{(1)} = \frac{1}{2} \pm \frac{t_f}{2}\text{arccosh}\left(\frac{2-T}{T}\right)$ and are symmetric around $\lambda = 1/2$. We recall that, in formula (74) the function $r_1(w)$ is given in Eq. (69) and $T = e^{-1/t_f}$. In Fig. 4 we plot both densities along with sample trajectories obtained by solving numerically the effective Langevin equations (33) and (36).

As already commented in the introduction, this solution for the special case $t = t_f/2$ appeared before in the literature in different contexts, including Chern–Simons theory and matrix models [25,26] as well as in the theory of Stieltjes–Wigert orthogonal polynomials [42], where this result in Eq. (74) was derived by different methods.

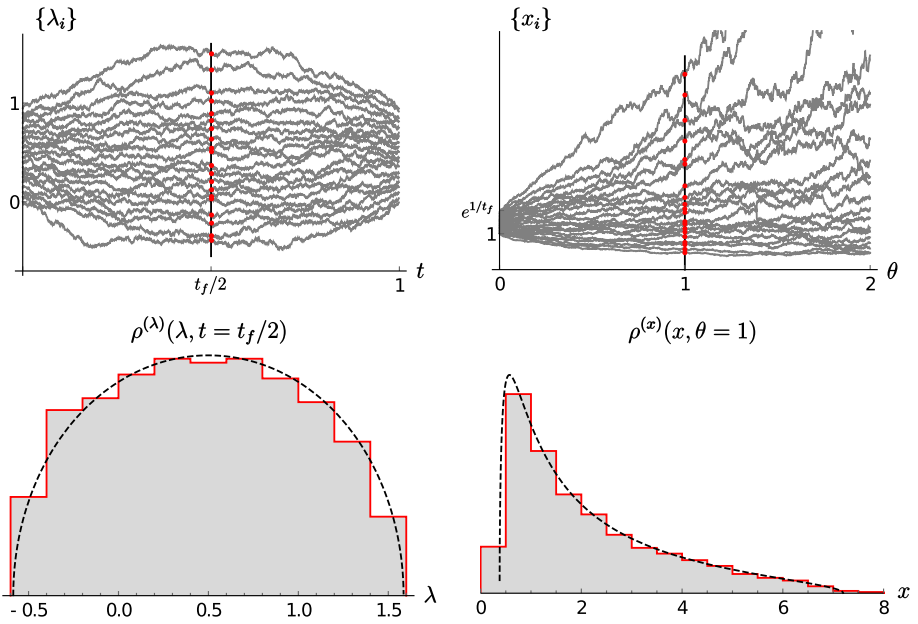

Fig. 4 Plots of sample trajectories and position densities in (λ, t) (left column) and (x, θ) (right column) variables for a flat-to-flat Brownian bridge. In the plots on the top we present sample trajectories as gray lines with black vertical line denoting the probing times $t = t_f/2$ and $\theta = 1$. For these times, we draw both analytic (dashed black line) and numeric (solid red line histograms) position densities given by formulas (73) and (74). Simulations were made for $t_f = 1$ and $N = 20$ by integrating the effective Langevin equations (33) and (36)

Given the explicit expressions for the average densities in (73) and (74), one can also compute the moments of the density. Indeed, in the case of the Gaussian ensembles of Random Matrix Theory, the moments of the Wigner semi-circle density have been computed explicitly in terms of Catalan numbers. We show in Appendix C that the Catalan numbers also appear for this density, albeit in a more complicated way.

4.3 Particle Densities for $t = \frac{2}{3}t_f$ and $t = \frac{3}{4}t_f$ ($\theta = 2$ and $\theta = 3$)

We turn to the study of other special cases where the solution to Eq. (67) is possible. We find indeed two special values $\theta = 2$ and $\theta = 3$ (corresponding to $t = \frac{2}{3}t_f$ and $t = \frac{3}{4}t_f$ respectively) where the equation for H (67) is cubic and quartic respectively and thus amenable to explicit solutions. In Fig. 5 we plot the densities for both times.

Average density for $t = 2t_f/3$. Using $\theta = t/(t_f - t)$, we see that this case corresponds to $\theta = 2$. Here, Eq. (67) for the e-Green's function is cubic and reads

$$wH^3 - wTH^2 - H + 1 = 0\,. \tag{75}$$

Three solutions of Eq. (75) are found by Cardano formulas [43] and the one with correct $w \to \infty$ behaviour $H \sim T$ is picked out:

$$H = \frac{T}{3} + \frac{e^{-i\pi/3}(3 + T^2 w)}{3R_2(w)^{1/3}} + \frac{e^{i\pi/3}R_2(w)^{1/3}}{3w}, \tag{76}$$

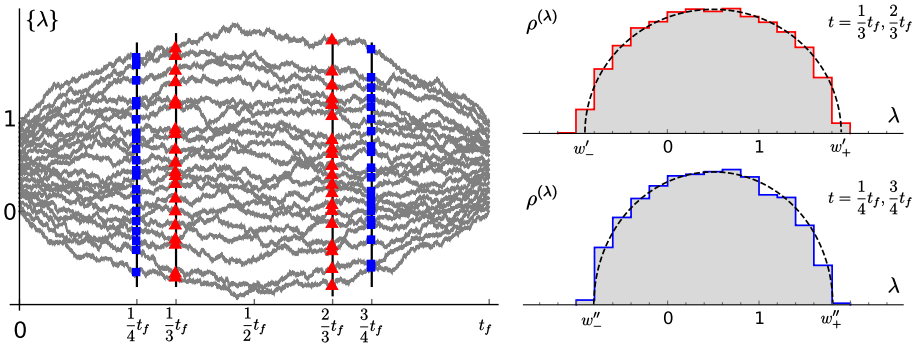

Fig. 5 The plot on the left shows sample trajectories as gray lines with red triangles denoting the positions at times $t = \frac{2}{3}t_f, \frac{1}{3}t_f$ and blue circles at times $t = \frac{3}{4}t_f, \frac{1}{4}t_f$. On the right we present both analytic (dashed black lines) and numeric (solid red line for $t = \frac{2}{3}t_f, \frac{1}{3}t_f$ and solid blue line for $t = \frac{3}{4}t_f, \frac{1}{4}t_f$) particle densities $\rho^{(\lambda)}$ given by formulas (79) and (82). Simulations were made for $t_f = 2$ and $N = 20$ by integrating the effective Langevin equations (33) and (36)

where $R_2(w) = (3Tw)^{3/2}\sqrt{r_2(w)} - (Tw)^3 + \frac{9}{2}(3-T)w^2$ and $r_2(w) = (w_+^{(2)} - w)(w - w_-^{(2)})$. The endpoints are given by $w_\pm^{(2)} = \frac{(3-T\pm\delta_2(T))(3-3T\pm\delta_2(T))^2}{2T^3(1-T\pm\delta_2(T))^2}$ with $\delta_2(T) = \sqrt{(9-T)(1-T)}$. We consider two cases depending on the endpoints $w_\pm^{(2)}$:

- For $x \notin (w_-^{(2)}, w_+^{(2)})$, the binomial $r_2(x) < 0$ and so the function $R_2(x)$ becomes complex. Despite that, the $H(x) > 0$ itself is a purely real and positive function. In that case, $\lim_{\epsilon\to 0_+} \arg H(x - i\epsilon) = 0$ and so the density vanishes $\rho^{(x)}(x; \theta = 2) = 0$.
- For $x \in (w_-^{(2)}, w_+^{(2)})$ (or when $r_2(x) > 0$) also $R_2(x) > 0$ and so the function is expanded

$$H(x - i\epsilon) = C_1' + iC_2' + \mathcal{O}(\epsilon^2), \tag{77}$$

where $C_1' = T/3 + \frac{3+T^2x}{6R_2(x)^{1/3}} + \frac{R_2(x)^{1/3}}{6x} + \mathcal{O}(\epsilon)$ and $C_2' = -\frac{\sqrt{3}(3+T^2x)}{6R_2(x)^{1/3}} + \frac{\sqrt{3}R_2(x)^{1/3}}{6x} + \mathcal{O}(\epsilon)$. The argument of H for $x \in (w_-^{(2)}, w_+^{(2)})$ is given by

$$\lim_{\epsilon\to 0_+} \arg H(x - i\epsilon) = \arctan\left(\frac{C_2'}{C_1'}\right).$$

We use formula (68) to find the particle density for $\theta = 2$:

$$\rho^{(x)}(x; \theta = 2) = \begin{cases} 0 & , \quad x \notin (w_-^{(2)}, w_+^{(2)}) \\ \frac{t_f}{\pi x} \arctan\left(\frac{\sqrt{3}\left[R_2(x)^{2/3} - x(3+T^2x)\right]}{x(3+T^2x) + 2TxR_2(x)^{1/3} + R_2(x)^{2/3}}\right) & , \quad x \in (w_-^{(2)}, w_+^{(2)}) \end{cases}. \tag{78}$$

Finally, the density in the λ-space is obtained from Eq. (39):

$$\rho^{(\lambda)}\left(\lambda; t = 2t_f/3\right) = \begin{cases} 0 & , \quad \lambda \notin (\lambda_-^{(2)}, \lambda_+^{(2)}) \\ \frac{3}{\pi} \arctan\left(\frac{\sqrt{3}\left[R_2(e^{3\lambda/t_f})^{2/3} - e^{3\lambda/t_f}(3+T^2e^{3\lambda/t_f})\right]}{e^{3\lambda/t_f}(3+T^2e^{3\lambda/t_f}) + 2Te^{3\lambda/t_f}R_2(e^{3\lambda/t_f})^{1/3} + R_2(e^{3\lambda/t_f})^{2/3}}\right) & , \quad \lambda \in (\lambda_-^{(2)}, \lambda_+^{(2)}) \end{cases}, \tag{79}$$

where the endpoints $\lambda_{\pm}^{(2)} = \frac{1}{2} \pm \frac{t_f}{3}\text{arccosh}\frac{9(3+2T)-T^2}{8T^{3/2}}$ with $T = e^{-1/t_f}$ and the function $R_2(w)$ is defined below Eq. (76). A plot of the density (79) is shown in the top-right plot of Fig. 5 and it is in very good agreement with the simulations results from the Langevin equations in (33).

Average density for $t = 3t_f/4$. This corresponds to $\theta = 3$, using $\theta = t/(t_f - t)$. In this case, the equation for the e-Green's function is quartic $wH^4 - wH^3 - H + 1 = 0$. The solution with correct asymptotic behaviour $H \sim T$ when $w \to \infty$ is given by Ferrari formulas [44]

$$H(w) = \frac{T}{4} + \frac{1}{2}\sqrt{S(w)} + \frac{1}{2}\sqrt{\frac{3T^2}{4} - S(w) + \frac{T^3 + 8/w}{4\sqrt{S(w)}}}, \tag{80}$$

where $S(w) = \frac{T^2}{4} + \frac{4-T}{3R_3(w)^{1/3}} + \frac{R_3(w)^{1/3}}{w}$, $R_3(w) = \frac{w}{2}\left(1 + wT^2 + T^2\sqrt{-r_3(w)}\right)$ and $r_3(w) = (w_+^{(3)} - w)(w - w_-^{(3)})$. The endpoints are now equal to $w_{\pm}^{(3)} = \frac{(2(1-T)\pm\delta_3(T))^3(2-T\pm\delta_3(T))}{T^4(1-T\pm\delta_3(T))^3}$ where $\delta_3(T) = \sqrt{(4-T)(1-T)}$. As before, we consider two cases.

- For $x \notin (w_-^{(3)}, w_+^{(3)})$ we argue that $H(x)$ is a real function. First, it is evident that the term $\sqrt{-r_3(x)} > 0$ is positive which results in both $R_3(x) > 0$ and $S(x) > 0$. These in turn render positive the functions under the square-roots of Eq. (80). As a consequence, the argument $\lim_{\epsilon \to 0_+} \arg H(x - i\epsilon) = 0$ is zero and the density vanishes:

$$\rho^{(x)}(x; \theta = 3) = 0\,, \qquad x \notin (w_-^{(3)}, w_+^{(3)}).$$

- For $x \in (w_-^{(3)}, w_+^{(3)})$, the square-root $\sqrt{-r_3(x)}$ becomes imaginary and so $R_3(x)$ is now complex. Still, $S(x)$ remains real and in the end only the square root part of $H(x)$ becomes imaginary which we take into account by setting $\sqrt{\frac{3T^2}{4} - S(w) + \frac{T^3+8/w}{4\sqrt{S(w)}}} = i\sigma\sqrt{-\frac{3T^2}{4} + S(w) - \frac{T^3+8/w}{4\sqrt{S(w)}}}$ where $\sigma = \pm 1$ encodes the branch. With this reformulation, the expansion (80) reads

$$H(x - i\epsilon) = \frac{T}{4} + \frac{1}{2}\sqrt{S(x)} + \frac{i\sigma}{2}\sqrt{-\frac{3T^2}{4} + S(x) - \frac{T^3 + 8/x}{4\sqrt{S(x)}}} + \mathcal{O}(\epsilon)$$

and so the argument of the function is simply $\lim_{\epsilon \to 0_+} \arg(H - i\epsilon) = \arctan\left(\frac{\sigma}{2}\frac{\sqrt{S(x) - \frac{3T^2}{4} - \frac{T^3+8/x}{4\sqrt{S(x)}}}}{T/4 + \frac{1}{2}\sqrt{S(x)}}\right)$.

We set $\sigma = -1$ to obtain a positive particle density

$$\rho^{(x)}(x; \theta = 3) = \begin{cases} 0 & , \quad x \notin (w_-^{(3)}, w_+^{(3)}) \\ \frac{t_f}{\pi x}\arctan\left(\frac{\sqrt{S(x)^{3/2} - \frac{3T^2}{4}S(x)^{1/2} - \frac{T^3}{4} - \frac{2}{x}}}{\frac{T}{2}S(x)^{1/4} + S(x)^{3/4}}\right) & , \quad x \in (w_-^{(3)}, w_+^{(3)})\,, \end{cases} \tag{81}$$

which in the λ-space is given by

$$\rho^{(\lambda)}\left(\lambda; t = 3t_f/4\right) = \begin{cases} 0 & , \quad \lambda \notin (\lambda_-^{(3)}, \lambda_+^{(3)}) \\ \frac{4}{\pi} \arctan\left(\frac{\sqrt{S\left(e^{4\lambda/t_f}\right)^{3/2} - \frac{3T^2}{4} S\left(e^{4\lambda/t_f}\right)^{1/2} - \frac{T^3}{4} - \frac{2}{e^{4\lambda/t_f}}}}{\frac{T}{2} S\left(e^{4\lambda/t_f}\right)^{1/4} + S\left(e^{4\lambda/t_f}\right)^{3/4}} \right) & , \quad \lambda \in (\lambda_-^{(3)}, \lambda_+^{(3)}) \, , \end{cases} \tag{82}$$

where $\lambda_\pm^{(3)} = \frac{1}{2} + \frac{t_f}{4} \text{arccosh} \frac{32(4-3T)-T^2(3+2T)}{27T^2}$ with $T = e^{-1/t_f}$ and where the function $S(w)$ is defined below Eq. (80). This formula is plotted in the bottom-right plot of Fig. 5 and shows excellent agreement with the simulations of the Langevin equations (33).

4.4 Support of the Density as a Function of Time

For generic value of the renormalised time θ, Eq. (67) for H is hard to solve to obtain the average density explicitly. However, one can still extract interesting information valid for any θ. In this subsection, we show how to compute the time evolution of the support of the average density by analysing the parametric solution (59) and (60) of the original Burgers' Eq. (48).

The edge of the average density can be extracted by adapting a method originally used in [38,45] for the DBM with $\beta = 2$ in the large N limit, which we discuss in detail in Appendix D. This method can be easily adapted to our problem, the only difference being that we work in (x, θ) coordinates, as opposed to the (λ, t) coordinates in the case of the $\beta = 2$ DBM (see Appendix D). We recall the parametric solution in Eqs. (59) and (60). For fixed y and θ we need to solve for ξ from the following equation

$$y = \xi + \theta \, G_0^{(x)}(\xi) \, . \tag{83}$$

Using the explicit expression of $G_0^{(x)}(\xi)$ from Eq. (64), we get

$$y = \xi + \theta \, \ln\left(\frac{e^\xi - 1}{T \, e^\xi - 1} \right) \, , \tag{84}$$

where we used $e^{-1/t_f} = T$. From Eqs. (83) and (84), we want to extract the edges at of the support of the average density $x_\pm(\theta)$ at "time" θ in the (x, θ)-coordinates. Adapting the method outlined in Appendix D for the $\beta = 2$ DBM, we can extract the edges of the support as follows.

In the complex ξ-plane, the function $y(\xi)$ in Eq. (84) has a cut along the real axis on the interval $\xi \in [0, 1/t_f]$. On this interval, $y(\xi)$ becomes purely imaginary, while it is real everywhere on the real ξ-axis outside this cut. In order to analyse the edges of the support of the density, we need to analyse the solution in the two intervals where $y(\xi)$ is real, namely $\xi \in (-\infty, 0]$ and $\xi \in [1/t_f, +\infty)$. The first interval $\xi \in (-\infty, 0]$ will give us information about the lower edge of the support of the average density, while the second interval $\xi \in [1/t_f, +\infty)$ provides information about the upper edge of the average density. For simplicity, we now focus on the second interval $\xi \in [1/t_f, +\infty)$ and derive the result for the upper edge $x_+(\theta)$ (in the (x, θ)-variables) and equivalently for $\lambda_+(t)$ (in the (λ, t)-variables).

The function $y(\xi)$, over the interval $\xi \in [1/t_f, +\infty)$, is plotted in Fig. 6. It diverges at the lower edge $\xi_{\text{edge}} = 1/t_f$ and increases linearly as $\xi \to \infty$. It clearly has a minimum at

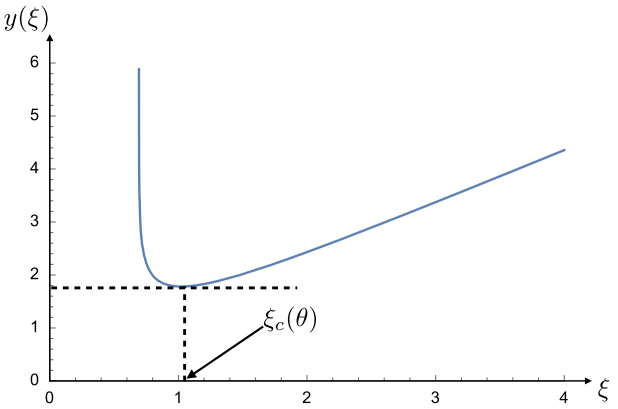

Fig. 6 Plot of $y(\xi)$ vs ξ, as given in Eq. (84), for $T = 1/2$ and $\theta = 1/2$. In this case $\xi_c(\theta) = \ln\left((7+\sqrt{17})/4\right) = 1.02273\ldots$, where the curve has its minimum

$\xi_c(\theta)$ which is determined by setting $dy/d\xi = 0$. This gives

$$1 + \theta\left(\frac{u}{u-1} - \frac{u\,T}{u\,T-1}\right) = 0 \quad \text{where} \quad u = e^{\xi_c(\theta)}\,. \tag{85}$$

This is a quadratic equation whose solutions are given by

$$u_{\pm}(\theta) = \frac{1}{2T}\left(1 + T + \theta(1-T) \pm \sqrt{(1+T+\theta(1-T))^2 - 4T}\right)\,. \tag{86}$$

Since $\xi_c(\theta) \in [1/t_f, +\infty)$, and $u = e^{\xi_c(\theta)}$, we must have $u(\theta) > 1/T$ where $T = e^{-1/t_f}$. This leads us to choose $u_+(\theta)$ as the correct root. We now have to substitute $\xi_c(\theta) = \ln u_+(\theta)$ in Eq. (84) to obtain the edge $y_c(\theta)$. For this it is convenient to first exponentiate the relation in Eq. (84) and rewrite it as

$$e^{y_c(\theta)} = u_+(\theta)\left(\frac{u_+(\theta)-1}{u_+(\theta)\,T-1}\right)^{\theta}\,. \tag{87}$$

Using $x_i = e^{y_i}$ then gives the upper boundary of the density in the (x, θ) coordinates

$$x_+(\theta) = e^{y_c(\theta)} = u_+(\theta)\left(\frac{u_+(\theta)-1}{u_+(\theta)\,T-1}\right)^{\theta}\,, \tag{88}$$

where $u_+(\theta)$ is given in Eq. (86). This concludes the derivation of the upper edge.

To compute the lower edge of the density, we need to repeat the same reasoning as above except that we have to consider instead the first interval $\xi \in (-\infty, 0]$. In this case, repeating the similar lines of reasoning, we actually arrive at the same equation (85). However, since $\xi_c(\theta) \in (-\infty, 0]$, we must have $u(\theta) = e^{\xi_c(\theta)} \in [0, 1]$ and indeed this is precisely given by the other root $u_-(\theta)$ of Eq. (86). It is easy to check from (86) that $u_-(\theta) \in [0, 1]$. This then gives us the lower edge of the support in the (x, θ) variables

$$x_-(\theta) = u_-(\theta)\left(\frac{u_-(\theta)-1}{u_-(\theta)\,T-1}\right)^{\theta}\,. \tag{89}$$

In Fig. 7 (right panel), we show a plot of these two boundaries $x_{\pm}(\theta)$ as a function of θ.

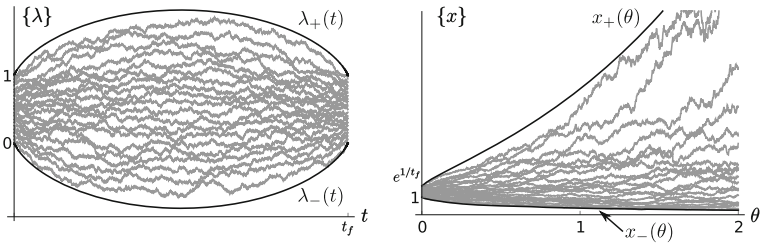

Fig. 7 Plot of sample trajectories (gray lines) in the (λ, t)-coordinates (left panel) and in the (x, θ)-coordinates (right panel). The solid lines correspond to the edges of the support of the average density. In the left panel, the lower (respectively upper) solid line corresponds to $\lambda_-(t)$ (respectively $\lambda_+(t)$) given in Eqs. (90). On the right panel, the lower solid line corresponds to $x_-(\theta)$ in Eq. (89), while the upper solid line corresponds to $x_+(\theta)$ in Eq. (88). Simulations were made for $t_f = 2$ and $N = 20$ by integrating the effective Langevin equations (33) and (36)

Now we can translate these results in terms of the (λ, t) coordinates, as defined in Eq. (35). Hence we set $\lambda_+(t) = \frac{t_f}{1+\theta}\, y_c(\theta)$ and $t = t_f \frac{\theta}{1+\theta}$ where $y_c(\theta)$ is given in Eq. (87). After a few steps of algebra, we can write $\lambda_+(t)$ explicitly. Similarly, for the lower support, we choose $u(\theta) = u_-(\theta)$ in Eq. (86) and replace $u_+(\theta)$ by $u_-(\theta)$ in Eq. (87). Repeating the same manipulations gives $\lambda_-(t)$. Together, they read

$$\lambda_\pm(t) = \frac{1}{2} \pm \left[t_f \operatorname{arccosh}\left(\frac{1}{\sqrt{T}} \frac{t_f + T(t_f - 2t)}{2(t_f - t)} \right) \right.$$
$$\left. - t \operatorname{arccosh}\left(\frac{(t_f - t)^2 + t^2 - T(t_f - 2t)^2}{2t(t_f - t)} \right) \right] \quad \text{where} \quad T = e^{-1/t_f} \,. \tag{90}$$

These boundaries $\lambda_\pm(t)$ are plotted in Fig. 7 (left panel). For the special values $\theta = 1, 2, 3$, i.e., $t = t_f/2, t_f/3$ and $t_f/4$ respectively, considered in the previous section, we recover the endpoints found in explicit formulae for the average density in Eqs. (73), (78) and (81).

Note that in this paper we have chosen the initial and the final flat configurations to have a unit density supported over the interval $[0, 1]$, i.e. $a_i = b_i = (i-1)/N$. One can easily generalise our results to the case where $a_i = b_i = \alpha(i-1)/N$ so that the initial and final densities are flat but with value $1/\alpha$ supported over the interval $[0, \alpha]$. We do not present the details here but we have verified that, taking the $\alpha \to 0$ limit with t_f fixed, we recover the known results for a pure "watermelon" configuration, where all the particles start at the origin at $t = 0$ and end up at the origin at $t = t_f$, i.e., "point to point" as opposed to "flat to flat" configurations. For example, we have checked that the formula for the boundaries of the support in Eq. (90), appropriately generalized to α, reduces, to leading order as $\alpha \to 0$, to

$$\lambda_\pm(t) = \pm \sqrt{\frac{4\alpha\, t\, (t_f - t)}{t_f}} \,, \tag{91}$$

which is exactly the boundary of a point-to-point watermelon with diffusion constant $D = \alpha/(2N)$ (see e.g. [14]).

4.5 Moments of the Average Density for Arbitrary Time $0 \le t \le t_f$

Another usefulness of the general result for H in Eq. (67) is that it allows to calculate the moments of the average density for arbitrary θ, which corresponds to arbitrary real time

Table 1 List of the five first moments of position density $\rho^{(x)}$ in the flat-to-flat Brownian bridge scenario valid for any time variable θ and obtained by iteratively solving Eq. (67)

k	$m^{(x)}_{k,\theta}/t_f$
0	$1/t_f$
1	$-(T-1)\,T^{-(\theta+1)}$
2	$\frac{1}{2}(T-1)T^{-2(\theta+1)}(-2\theta+(2\theta-1)T-1)$
3	$-\frac{1}{6}(T-1)T^{-3(\theta+1)}\left(9\theta^2+9\theta+\left(9\theta^2-9\theta+2\right)T^2+\left(2-18\theta^2\right)T+2\right)$
4	$\frac{1}{12}(T-1)T^{-4(\theta+1)}\Big(-32\theta^3-48\theta^2-22\theta+\left(32\theta^3-48\theta^2+22\theta-3\right)T^3$ $+\left(-96\theta^3+48\theta^2+6\theta-3\right)T^2$ $+\left(96\theta^3+48\theta^2-6\theta-3\right)T-3\Big)$
5	$-\frac{1}{120}(T-1)T^{-5(\theta+1)}\Big(625\theta^4+1250\theta^3+875\theta^2+250\theta$ $+\left(625\theta^4-1250\theta^3+875\theta^2-250\theta+24\right)T^4$ $-4\left(625\theta^4-625\theta^3+125\theta^2+25\theta-6\right)T^3$ $+6\left(625\theta^4-125\theta^2+4\right)T^2$ $-4\left(625\theta^4+625\theta^3+125\theta^2-25\theta-6\right)T+24\Big)$

through the relation $t=\theta\, t_f/(1+\theta)$. To compute this, we recall the definition of the Green's function given by Eq. (40) (with $e^z=w$) and expand it in power of $1/w$

$$G^{(x)}(z;\theta)=\frac{1}{t_f}\sum_{k=0}^{\infty}\frac{m^{(x)}_{k,\theta}}{w^k}, \tag{92}$$

where $m^{(x)}_{k,\theta}=\int dx x^k\rho^{(x)}(x;\theta)$ are the moments of the density. We plug $H=e^{-G^{(x)}}$ into the solution (67) and expand in powers of $1/w$. By matching the powers of $1/w$ on both sides of (67), we obtain a recursion relation between the moments which can then be used to compute the moments successively. We list the first few moments in Table 1. We cross-checked the algorithm up to 10-th order with explicit moment formulas $m^{(x)}_{k,\theta=1}$, for $\theta=1$, given by Eq. (C2).

5 VBB and Its Relation to Other Models

Flat-to-flat VBB as described in the present work is also related to other models. We discuss briefly connections to Chern–Simons matrix model, biorthogonal Stieltjes–Wigert ensemble and Muttalib-Borodin ensemble.

We recall that the joint distribution of the positions $\vec{\lambda}$ of N particles in the VBB at time t is given in Eq. (4) where $P_{\mathrm{VBM},D}$ is given by the Karlin-McGregor formula in Eq. (27). Setting $D=1/(2N)$ in Eq. (4) we then get

$$P_{\mathrm{VBB},D=\frac{1}{2N}}\left(\vec{\lambda},t|\vec{a},0;\vec{b},t_f\right)\propto \det_{1\le i,j\le N}\left(e^{-\frac{N}{2t}(\lambda_i-a_j)^2}\right)\det_{1\le i,j\le N}\left(e^{-\frac{N}{2(t_f-t)}(b_i-\lambda_j)^2}\right), \tag{93}$$

where we keep track of only the λ-dependent terms. In the case of flat initial and final positions $a_i = b_i = \frac{i-1}{N}$ we obtain

$$P_{\mathrm{VBB},D=\frac{1}{2N}}\left(\vec{\lambda},t|\vec{a},0;\vec{b},t_f\right)\propto\prod_{i=1}^{N}e^{-\frac{Nt_f}{2t(t_f-t)}\lambda_i^2+\frac{(N-1)t_f}{2t(t_f-t)}\lambda_i}\prod_{i>j}$$
$$\times\sinh\left(\frac{\lambda_i-\lambda_j}{2t}\right)\prod_{i>j}\sinh\left(\frac{\lambda_i-\lambda_j}{2(t_f-t)}\right). \tag{94}$$

The pdf is not symmetric under the exchange $\lambda_i \to -\lambda_i$ as both initial and final conditions lack this symmetry. On the other hand, time reversal symmetry $t \to t_f - t$ is preserved. Performing the shift $\lambda_i \to \lambda_i - \frac{N-1}{2N}$ and setting $t = t_f/2$, the rhs of (94) reduces exactly, up to a global proportionality factor, to the statistical weight factor appearing in the partition function of the Chern–Simons model [25,26], and is also related to the theory of Stieltjes–Wigert orthogonal polynomials [27–30]. For other values of t, the rhs can be identified with the statistical weight in a generalized Chern–Simons model and also can be related to the theory of bi-orthogonal Stieltjes–Wigert polynomials [27,28].

There is yet another way of rewriting the joint distribution $P_{\mathrm{VBB},D=\frac{1}{2N}}$ in (93). For the flat initial conditions $a_i = b_i = (i-1)/N$, one can evaluate the determinant as in Eqs. (28) and (31). In terms of the variables $x_i = e^{\theta\lambda_i/t}$ and $\theta = t/(t_f - t)$, the joint distribution can be expressed as

$$\mathcal{P}_{\mathrm{VBB},D=\frac{1}{2N}}\left(\vec{x},\theta|\vec{a},0;\vec{b},t_f\right)\propto\prod_{i=1}^{N}e^{-\frac{Nt_f}{2\theta}(\log x_i)^2-\log x_i}\prod_{i>j}(x_i-x_j)\prod_{i>j}\left(x_i^{1/\theta}-x_j^{1/\theta}\right). \tag{95}$$

Thus in terms of the (x,θ) variables, the VBB joint distribution is also related to Muttalib-Borodin ensemble [46,47] with parameter $1/\theta$.

Comparison with finite N results. Establishing relations with other models enables some comparisons. Asymptotic results established in present work are juxtaposed with a closed form of the particle densities $\rho_N^{(x)}$ valid for finite N:

$$\rho_N^{(x)}(x;\tau,q)=\frac{1}{qN}w(x/q,q)\sum_{n=0}^{N-1}T_n(x/q,\tau,q)R_n(x/q,\tau,q), \tag{96}$$

where the weight $w(x,q)=\frac{1}{\sqrt{2\pi|\log q|}}\exp\left(-\frac{(\log x)^2}{2|\log q|}\right)$ and the polynomials read

$$T_n(x,\tau,q)=(-1)^n\frac{\sqrt{(q;q)_n}q^{(n\tau+1/2)/2}}{(q^\theta;q^\theta)_n}\sum_{l=0}^{n}(-1)^l\begin{bmatrix}n\\l\end{bmatrix}_{q^\tau}q^{\tau l(l(\tau+1)+1)/2}x^{\tau l},$$
$$R_n(x,\tau,q)=(-1)^n\frac{q^{(n\tau+1/2)/2}}{\sqrt{(q;q)_n}}\sum_{l=0}^{n}(-1)^l\begin{bmatrix}n\\l\end{bmatrix}_{q^\tau}q^{l(l(\tau+1)+(1-\tau)+1)/2}x^l, \tag{97}$$

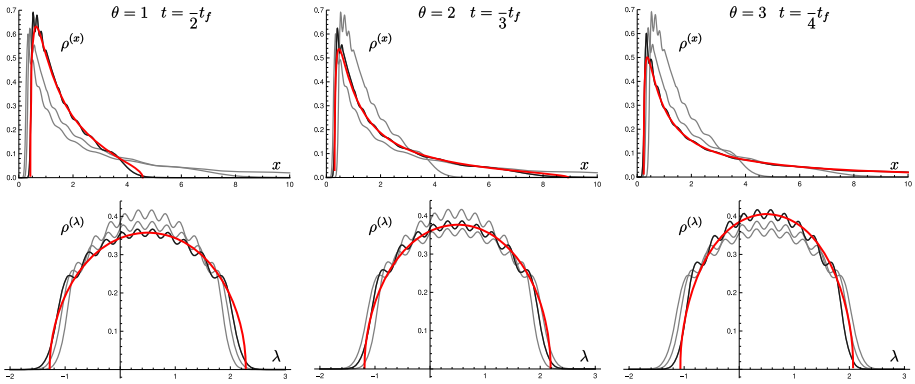

Fig. 8 Plots of exact position density given by Eq. (96) and asymptotic formulas (73),(78) and (81) for times $\theta = 1, 2, 3$ (or $t = \frac{1}{2}t_f, \frac{2}{3}t_f, \frac{3}{4}t_f$). The asymptotic formulas show no oscillatory behaviour, otherwise the matching is very good even for moderate number of particles. The plots were made for $N = 10$ and $t_f = 3$

where $\begin{bmatrix} x \\ y \end{bmatrix}_q$ and $(q;q)_n$ are the q-extensions of the binomial and the Pochhammer symbol respectively. The formula can be found in Eq. (62) of [29] where only a proper rescaling was introduced to correct the (lack of) symmetry in the joint distribution of the VBB (95).

In our notation, the q and τ parameters are equal to $q = e^{-\frac{\theta}{Nt_f}}$ and $\tau = \frac{1}{\theta}$ respectively. The formula in (96) is therefore the particle density in the (x, θ) space and the transformation to (λ, t) variables is given by Eq. (39). In Fig. 8 we present comparison between asymptotic density formulas valid for times $\theta = 1, 2, 3$ found in Eqs. (73), (78) and (81) with an exact formula (96).

Kernel structure of the underlying determinantal process. Finally, we end this section by making some remarks on the form of the kernel that characterises the determinantal process. The formulae provided below are perhaps a bit formal but they maybe be useful for future large N asymptotic analysis. A general reader may skip this section, which is intended for experts in the field.

We start with the joint pdf (95) itself

$$P_{\tau,q} \sim \prod_{i=1}^{N} e^{-\frac{(\log x_i)^2}{2|\log q|} - \log x_i} \prod_{i>j} (x_i - x_j) \prod_{i>j} \left(x_i^{\tau} - x_j^{\tau} \right),$$

where we reintroduced the parameters q, τ. Our aim is to offer an integral representation of the kernel complementing the density formula (96). To this end, we cast the jpdf into a biorthogonal form

$$P_{\tau,q} \sim \det\left(\eta_i(x_j)\right)_{i,j=1\ldots N} \det\left(\xi_i(x_j)\right)_{i,j=1\ldots N},$$

where the polynomials are $\eta_i(x) = x^{i-1}$ and $\xi_i(x) = \frac{1}{\sqrt{2\pi|\log q|}} e^{-\frac{(\log x)^2}{2|\log q|} - \log x} x^{\tau(i-1)}$. The following formula found in [48] gives the kernel function simply related to the average of ratio of determinants

$$\left\langle \prod_{i=1}^{N} \frac{v - x_i}{z - x_i} \right\rangle = \int_0^{\infty} dx \frac{v - x}{z - x} K_N(v, x). \tag{98}$$

To calculate the ratio we use the following formula given in [49,50]:

$$\left\langle \prod_{i=1}^{N} \frac{v-x_i}{z-x_i} \right\rangle = \int_0^\infty dx \frac{v-x}{z-x} \sum_{k=1}^{N} \xi_k(x) \frac{\det g_k(v)}{\det g}, \tag{99}$$

where the matrix elements are $g_{ij} = \int_0^\infty dx \eta_i(x)\xi_j(x) = q^{-\frac{1}{2}[i-1+\tau(j-1)]^2}$ and the matrix $g_k(v)$ is g with k-th column replaced by a vector $(1, v, ..., v^{N-1})$. Since the elements g_{ij} are quadratic function of the indices, we can rewrite both determinants as Vandermonde terms. To cast the v-dependent column into a form compatible with the Vandermonde structure, we use an integral representation of the monomial function $v^{n-1} = \frac{q^{-n^2/2+n(\tau+1)}}{v\sqrt{2\pi|\log q|}} \int_{-\infty}^{\infty} dw e^{-\frac{(w+i\log\frac{v}{q^{\tau+1}})^2}{2|\log q|}+inw}$. Using these manipulations, we can rewrite the ratio of determinants as

$$\frac{\det g_k(v)}{\det g} = \frac{1}{vk_k\mu_k\sqrt{2\pi|\log q|}} \int_{-\infty}^{\infty} dw e^{-\frac{(w+i\log\frac{v}{q^{\tau+1}})^2}{2|\log q|}+iw} \prod_{j(\neq k)} \frac{\mu_j - e^{iw}}{\mu_j - \mu_k}, \tag{100}$$

with $k_j = q^{-\frac{1}{2}(\tau(j-1)-1)^2}$ and $\mu_j = q^{-\tau j}$. In the last step, we extract the k-dependent terms from formula (100) and introduce the sum

$$S = \sum_{k=1}^{N} \frac{\xi_k(x)}{k_k\mu_k} \prod_{j(\neq k)} \frac{\mu_j - e^{iw}}{\mu_j - \mu_k}.$$

We plug in the definitions and insert the index $k = -\frac{\log\mu_k}{\tau\log q}$ obtained by inverting the definition of μ_k. This results in a sum which can be expressed through a contour integral

$$S = -\frac{e^{-\frac{(\log x)^2}{2|\log q|}-\log x}}{\sqrt{2\pi|\log q|}} \oint_C \frac{du}{2\pi i} x^{-\tau\left(\frac{\log u}{\tau\log q}+1\right)} q^{\frac{\left[\tau\left(\frac{\log u}{\tau\log q}+1\right)+1\right]^2}{2}} \frac{1}{u(u-e^{iw})} \prod_{j=1}^{N} \frac{e^{iw}-\mu_j}{u-\mu_j}, \tag{101}$$

where the contour C encircles anti-clockwise all poles located at μ_j's but stays outside both 0 and e^{iw}. We bring together Eqs. (99) and (101) and use the formula (98):

$$K_N(x,y) = \frac{1}{2\pi|\log q|x} \oint_C \frac{du}{2\pi i} \int_{-\infty}^{\infty} dw e^{-\frac{\left[w+i\log\left(x/q^{\tau+1}\right)\right]^2+\left[\log u-\log\left(y/q^{\tau+1}\right)\right]^2}{2|\log q|}} \frac{e^{iw}}{u(e^{iw}-u)} \prod_{j=1}^{N} \frac{e^{iw}-q^{-j\tau}}{u-q^{-j\tau}}. \tag{102}$$

The particle density is the diagonal part of the kernel. Equivalence with Eq. (96) can be established by an identity $\frac{1}{e^{iw}-u)} \prod_{j=1}^{N} \frac{e^{iw}-q^{-j\tau}}{u-q^{-j\tau}} = \frac{1}{e^{iw}-u} + \sum_{n=0}^{N-1} \frac{\prod_{j=1}(e^{iw}-q^{-j\tau})}{\prod_{j=1}^{n+1}(u-q^{-j\tau})}$. The first term in this identity is vanishing due to the contour integral. Integrals in the remaining sum are decoupled and form integral representations of the polynomials defined by Eqs. (97). The coupled form (102) is however a promising step in conducting asymptotic analysis independently of the Dysonian approach presented in this work. For completeness, the kernels in both (λ, t) and (x, θ) variables are found by setting $q = e^{-\frac{\theta}{Nt_f}}$ and $\tau = 1/\theta$ and using Eq. (35)

$$K_N^{(x)}(x,y;\theta) = \frac{Nt_f}{2\pi\theta x}\int_{-\infty}^{\infty} dw \oint_C \frac{du}{2\pi i} e^{-\frac{Nt_f}{2\theta}\left[\left(w+i\log x+i\frac{\theta+1}{Nt_f}\right)^2+\left(\log u-\log y-\frac{\theta+1}{Nt_f}\right)^2\right]} \frac{e^{iw}}{u(e^{iw}-u)}\prod_{j=1}^{N}\frac{e^{iw}-e^{\frac{j}{Nt_f}}}{u-e^{\frac{j}{Nt_f}}}, \tag{103}$$

$$K_N^{(\lambda)}(\xi,\lambda;t) = \frac{Nt_f}{2\pi t}\int_{-\infty}^{\infty} dw \oint_C \frac{du}{2\pi i} e^{-\frac{Nt_f(t_f-t)}{2t}\left[\left(w+i\frac{\xi+N^{-1}}{t_f-t}\right)^2+\left(\log u-\frac{\lambda+N^{-1}}{t_f-t}\right)^2\right]} \frac{e^{iw}}{u(e^{iw}-u)}\prod_{j=1}^{N}\frac{e^{iw}-e^{\frac{j}{Nt_f}}}{u-e^{\frac{j}{Nt_f}}}, \tag{104}$$

where the densities read simply $\rho_N^{(\lambda)}(\lambda;t) = \frac{1}{N}K_N^{\lambda)}(\lambda,\lambda;t)$ and $\rho_N^{(x)}(x;\theta) = \frac{1}{N}K_N^{(x)}(x,x;\theta)$. These kernels form the basic building blocks to compute the correlation functions in the model described by (94) and (95).

6 Summary and Outlook

In this paper, we have studied N vicious Brownian bridges propagating from an initial configuration $\vec{a}$ at time $t = 0$ to a final configuration $\vec{b}$ at time $t = t_f$, while staying non-intersecting for all $0 \le t \le t_f$. We mapped this vicious bridge problem exactly to Dyson's Brownian bridges with Dyson index $\beta = 2$ and for the latter we derived an exact effective Langevin equation that generates very efficiently the vicious bridge configurations. In particular, for the flat-to-flat configuration in the large N limit, we used this Langevin equation to derive an exact Burgers' equation (in the inviscid limit) for the Green's function and provided the solution of this Burgers' equation at arbitrary time $0 \le t \le t_f$. We emphasize that this Burgers' equation is derived from the effective Langevin equation for the bridge in the transformed (x,θ) coordinates [see Eq. (36)] and already contains in it the future information about the final bridge condition at $t = t_f$. In this sense, this is different from the canonical Burgers' equation associated to the $\beta = 2$ DBM, which is well known. From this Burgers' equation, we were able to derive the average density of the flat-to-flat bridge explicitly at certain specific values of intermediate times t, such as $t = t_f/2$, $t = t_f/3$ and $t = t_f/4$. We also derive explicitly how the two edges of the average density evolve from time $t = 0$ to time $t = t_f$. Finally, we made links to other well studied problems, such as the Chern–Simons model, the related Stieltges-Wigert orthogonal polynomials and the Borodin–Muttalib ensemble of determinantal point processes.

We remark that there exists a well known simple case of the vicious Brownian bridges where both the initial ($t = 0$) and the final ($t = t_f$) configurations have densities given by the Wigner semi-circular law. In this "Wigner-to-Wigner" case, it is easy to see that the average density at all intermediate times remains a Wigner semi-circle (with a time dependent rescaling). This is because under the evolution via Dyson's Brownian motion $\beta = 2$ the average density remains a semi-circle if the initial density is itself a Wigner semi-circle. In this paper, our result for the flat-to-flat geometry for the VBB provides another example where one can make analytical progress. It would be of course very interesting to see if the VBB problem can be solved for other initial and final positions of the particles. This will be particularly useful to compute the large N asymptotics of the Harish-Chandra-Itzykson-Zuber integral (for $\beta = 2$) connecting arbitrary matrices A and B [32,51].

Finally, our work derives the effective Langevin equation for vicious bridge configurations, thus generalising the single particle effective Langevin equation for a bridge [5] to an interacting many-body system. In fact, in the single particle setting, an effective Langevin equation was derived not just for the bridge configuration but also for other constrained walks such as the Brownian excursion, the Brownian meander, etc. It would be interesting to extend the approach presented here for the many-particle vicious bridges to that of vicious excursions or meanders.

Acknowledgements We thank J.-P. Bouchaud, J. Bun, P. Mergny, H. Orland and M. Potters for useful discussions. This research was supported by ANR grant ANR-17-CE30-0027-01 RaMaTraF. JG acknowledges support by the TEAMNET POIR.04.04.00- 00-14DE/18-00 grant of the Foundation for Polish Science.

Appendix A: Derivation of Eq. (43)

We recall the definition of characteristic polynomial (42) and formulate its "non-averaged" version

$$\tilde{\Omega}_N(y) = \prod_{i=1}^{N} \left(e^y - x_i\right).$$

The positions x_i evolve according to the Langevin equation (36) which is rewritten as the following stochastic differential equation (hereafter SDE)

$$dx_i = \frac{1}{Nt_f} \sum_{j(\neq i)} \frac{x_i^2}{x_i - x_j} d\theta + \frac{1+\theta}{t_f} x_i dW_i \ , \tag{A1}$$

where the Wiener process is defined by $dW_i dW_j = \delta_{ij} \frac{1}{N} d\theta$. We compute the evolution equation for $\tilde{\Omega}_N(y)$ under the stochastic motion (A1). To this end, we use Ito's lemma

$$d\tilde{\Omega}_N = \sum_i \frac{\partial \tilde{\Omega}_N}{\partial x_i} dx_i + \frac{1}{2} \sum_{i,j} \frac{\partial^2 \tilde{\Omega}_N}{\partial x_i \partial x_j} dx_i dx_j \ . \tag{A2}$$

We compute the derivatives as

$$\frac{\partial \tilde{\Omega}_N}{\partial x_i} = -\frac{\tilde{\Omega}_N}{e^y - x_i} \ ,$$
$$\frac{\partial^2 \tilde{\Omega}_N}{\partial x_i \partial x_j} = 0 \ ,$$

and find

$$\sum_i \frac{\partial \tilde{\Omega}_N}{\partial x_i} dx_i = -\tilde{\Omega}_N \left(\frac{N-1}{Nt_f} d\theta \sum_i \frac{x_i}{e^y - x_i} + \frac{1}{Nt_f} d\theta \sum_{j(\neq i)} \frac{x_i x_j}{(e^y - x_i)(x_i - x_j)} \right.$$
$$\left. + \frac{1+\theta}{Nt_f} \sum_i \frac{x_i dW_i}{e^y - x_i} \right),$$
$$\sum_{i,j} \frac{\partial^2 \tilde{\Omega}_N}{\partial x_i \partial x_j} dx_i dx_j = 0 \ . \tag{A3}$$

To obtain a closed equation, each term in the above expression ought to be expressed in terms of $\tilde{\Omega}_N$. To this end, we compute first partial results

$$\partial_y \tilde{\Omega}_N = e^y \tilde{\Omega}_N \sum_i \frac{1}{e^y - x_i},$$
$$\partial_{yy} \tilde{\Omega}_N - \partial_y \tilde{\Omega}_N = \tilde{\Omega}_N \sum_{i \neq j} \frac{e^{2y}}{(e^y - x_i)(e^y - x_j)},$$

and use them to get

$$\sum_i \frac{x_i}{e^y - x_i} = -N + e^y \sum_i \frac{1}{e^y - x_i} = -N + \frac{\partial_y \tilde{\Omega}_N}{\tilde{\Omega}_N}, \tag{A4}$$
$$\sum_{i \neq j} \frac{x_i x_j}{(e^y - x_i)(x_i - x_j)} = \frac{N(N-1)}{2} + e^y (N-1) \sum_i \frac{1}{x_i - e^y} + \frac{e^{2y}}{2} \sum_{i \neq j} \frac{1}{(x_i - e^y)(x_j - e^y)}$$
$$= \frac{N(N-1)}{2} - (N-1) \frac{\partial_y \tilde{\Omega}_N}{\tilde{\Omega}_N} + \frac{\partial_{yy} \tilde{\Omega}_N}{2\tilde{\Omega}_N} - \frac{\partial_y \tilde{\Omega}_N}{2\tilde{\Omega}_N}, \tag{A5}$$

which are plugged back into Eq. (A3) and (A2) to yield

$$d\tilde{\Omega}_N = \frac{N-1}{2t_f} \tilde{\Omega}_N d\theta + \frac{1}{2Nt_f} \left(\partial_y \tilde{\Omega}_N - \partial_{yy} \tilde{\Omega}_N \right) d\theta - \frac{1+\theta}{Nt_f} \tilde{\Omega}_N \sum_i \frac{x_i dW_i}{e^y - x_i}.$$

This is a closed equation for $\tilde{\Omega}_N$ and the stochastic part is proportional to dW_i. This thus drops out when looking at the averaged characteristic polynomial $\langle \tilde{\Omega}_N \rangle = \Omega_N$, i.e.,

$$\partial_\theta \Omega_N = \frac{N-1}{2t_f} \Omega_N + \frac{1}{2Nt_f} \left(\partial_y \Omega_N - \partial_{yy} \Omega_N \right),$$

which is exactly the Eq. (43) given in the text.

Appendix B: Derivation of Eq. (68)

We start from the Sochocki–Plemejl formula relating the particle density and the e-Green's function H

$$\rho^{(x)}(x, \theta) = -\frac{t_f}{\pi} \lim_{\epsilon \to 0_+} \mathrm{Im} \left[\frac{1}{w} \ln H(w; \theta) \right]_{w = x - i\epsilon}. \tag{B1}$$

We use the complex logarithm formula

$$\ln(H(x - i\epsilon)) = \ln |H(x - i\epsilon)| + i \arg H(x - i\epsilon)) + 2k\pi i \ ,$$

where k enumerates the branch cuts of the logarithm and where the real and imaginary parts are clearly separated. We also expand $1/(x - i\epsilon) = \frac{x + i\epsilon}{x^2 + \epsilon^2}$, plug these two formulas into Eq. (B1) and find

$$\rho^{(x)}(x, \theta) = -\frac{t_f}{\pi} \lim_{\epsilon \to 0_+} \left[\frac{\epsilon \ln |H(x - i\epsilon)|}{x^2 + \epsilon^2} + \frac{x}{x^2 + \epsilon^2} (\arg H(x - i\epsilon) + 2k\pi) \right].$$

We assume that $\frac{\epsilon \ln|H(x-i\epsilon)|}{x^2+\epsilon^2} \to 0$ as $\epsilon \to 0$ and we are left with

$$\rho^{(x)}(x,\theta) = -\frac{t_f}{\pi} \lim_{\epsilon\to 0_+} \left[\frac{x}{x^2+\epsilon^2} (\arg H(x-i\epsilon) + 2k\pi) \right] .$$

We choose the branch $k = 0$ to make the resulting density normalizable (i.e. not divergent) and for $x > 0$ the term $x/(x^2+\epsilon^2)$ is regular and can be safely taken out of the limit which finally gives Eq. (68).

Appendix C: Calculation of the Moments of the average density for $t = t_f/2$.

In this Appendix we compute the moments of the densities $\rho^{(x)}$ in Eq. (73) and $\rho^{(\lambda)}$ in Eq. (74). We start with $\rho^{(x)}$ and set $w_\pm^{(1)} = x_\pm$ in Eq. (73). The k-th moment of the average density, using Eq. (73), is then given by

$$m^{(x)}_{k,\theta=1} = \int_{x_-}^{x_+} dx\, x^k \rho^{(x)}(x;\theta=1) = \frac{t_f}{\pi} \int_{x_-}^{x_+} dx\, x^{k-1} \arctan\left[\frac{\sqrt{4x-(1+xT)^2}}{1+xT} \right] \quad \text{(C1)}$$

We perform a change of variables $x = \frac{1}{T}\left(\frac{2}{T}\left(1+\sqrt{1-T}\,p\right)-1\right), dx = \frac{2\sqrt{1-T}}{T^2} dp$ resulting in

$$m^{(x)}_{k,\theta=1} = \frac{2t_f\sqrt{1-T}}{\pi T^{2k}} \int_{-1}^{1} dp \left(2p\sqrt{1-T}+2-T\right)^{k-1} \arctan\left(\frac{\sqrt{1-T}\sqrt{1-p^2}}{1+\sqrt{1-T}\,p} \right).$$

We continue with integration by parts. Since by normalization the zeroth moment is unity $m^{(x)}_{0,\theta=1} = 1$, we continue with $k \geq 1$ for which the following formula holds:

$$m^{(x)}_{k,\theta=1} = -\frac{t_f(2\sqrt{1-T})^{k-1}}{k\pi T^{2k}} \sum_{n=0}^{k-1} \binom{k-1}{n} \left(\frac{2-T}{2\sqrt{1-T}}\right)^{k-1-n} \left[(T-1)J_n - \sqrt{1-T}\,J_{n+1} \right],$$

where $J_n = \int_{-1}^{1} dp\, p^n/\sqrt{1-p^2}$. These integrals are expressible via Catalan numbers $C_n = \frac{1}{n+1}\binom{2n}{n}$ since $J_0 = \pi$, $J_{2n} = \frac{2\pi(2n-1)}{4^n} C_{n-1}$ and $J_{2n-1} = 0$ for $n > 0$:

$$\begin{aligned} m^{(x)}_{k,\theta=1} = {} & \frac{t_f(1-T)(2-T)^{k-1}}{kT^{2k}} + \frac{2t_f(1-T)^2(2-T)^{k-3}}{kT^{2k}} \\ & \sum_{n=0}^{\lfloor\frac{k-1}{2}\rfloor-1} \binom{k-1}{2n+2} \left(\frac{\sqrt{1-T}}{2-T}\right)^{2n} (2n+1)C_n + \\ & + \frac{t_f(1-T)(2-T)^{k-2}}{kT^{2k}} \sum_{n=0}^{\lfloor\frac{k}{2}-1\rfloor} \binom{k-1}{2n+1} \left(\frac{\sqrt{1-T}}{2-T}\right)^{2n} (2n+1)C_n \,. \end{aligned} \quad \text{(C2)}$$

Thus, interestingly, the Catalan numbers also appear here.

An alternative formulation of these moments in terms of the modified Bessel function is possible with the use of an identity $\int_{-1}^{1} dp \frac{e^{-\alpha p}}{\sqrt{1-p^2}} = \pi I_0(\alpha)$ applied to the integrals $J_n = (-1)^n \lim_{\alpha\to 0} \frac{\partial^n}{\partial\alpha^n} \int_{-1}^{1} dp \frac{e^{-\alpha p}}{\sqrt{1-p^2}}$. We find:

$$m_{k,\theta=1}^{(x)} = \frac{t_f a(-2)^{k-1}}{kT^{2k}} \frac{\partial^{k-1}}{\partial \alpha^{k-1}} \left[e^{-\frac{\alpha(2-T)}{2}} \left(a I_0(\alpha a) - I_1(\alpha a) \right) \right]_{\alpha=0}, \qquad k \geq 1,$$

where $a = \sqrt{1-T}$ and $I_i(x)$ is the modified Bessel function.

Using the relation (39) between particle densities in x and λ spaces, we translate the moments find

$$\begin{aligned} m_{k,\theta=1}^{(\lambda)} &= \int_{\lambda_-}^{\lambda_+} d\lambda \lambda^k \rho^{(\lambda)}(\lambda; \theta = 1) \\ &= \frac{t_f}{\pi} \left(\frac{t_f}{2} \right)^k \int_{x_-}^{x_+} \frac{dx}{x} (\log x)^k \arctan \left(\frac{\sqrt{4x - (1+xT)^2}}{1+xT} \right). \end{aligned}$$

We again change the variables:

$$m_{k,\theta=1}^{(\lambda)} = \frac{t_f a}{2\pi(k+1)} \left(\frac{t_f}{2} \right)^k \int_{-1}^{1} dp \frac{(c + \log(ap+b))^{k+1}(a+p)}{(ap+b)\sqrt{1-p^2}},$$

with $a = \sqrt{1-T}, b = 1 - T/2, c = \log 2 + 2/t_f$. Now with the identity $\int_{-1}^{1} dp \frac{1}{(ap+b)^\alpha \sqrt{1-p^2}} = \frac{\pi}{\sqrt{b^2-a^2}^\alpha} P_\alpha \left(\frac{b}{\sqrt{b^2-a^2}} \right)$ where P_α is a Legendre function, the moments in λ space are given by:

$$m_{k,\theta=1}^{(\lambda)} = \frac{t_f(-1)^{k+1}}{2(k+1)} \left(\frac{t_f}{2} \right)^k \frac{\partial^{k+1}}{\partial \alpha^{k+1}} \left[T^\alpha \left(P_{\alpha-1} \left(\frac{2-T}{T} \right) - P_\alpha \left(\frac{2-T}{T} \right) \right) \right]_{\alpha=0}.$$

As a last step, we propose a general identity (found only in special case $n = 2$ in eq. 1.9 of [52] but checked by us numerically in Mathematica for n up to 5):

$$\frac{\partial^n}{\partial \alpha^n} \left[P_{\alpha-1}(x) - P_\alpha(x) \right]_{\alpha=0} = \begin{cases} 0, & n \text{ is even} \\ -2 \frac{\partial^n}{\partial \alpha^n} P_\alpha(x)_{\alpha=0}, & n \text{ is odd,} \end{cases},$$

which renders the final expression:

$$m_{k,\theta=1}^{(\lambda)} = \frac{t_f}{(k+1)} \left(-\frac{t_f}{2} \right)^k \sum_{l=0}^{\left\lfloor \frac{k+1}{2} \right\rfloor} \binom{k+1}{l} (\log T)^{k-2l} \frac{\partial^{2l+1}}{\partial \alpha^{2l+1}} \left(P_\alpha \left(\frac{2-T}{T} \right) \right)_{\alpha=0} \quad \text{(C3)}$$

Although the expression for the moments in the x-space in (C2) is easy to evaluate numerically, evaluating explicitly the moments in the λ-space from Eq. (C3) is difficult due to the apparent lack of explicit formulae for the derivatives of the Legendre function with respect to its degree (see e.g. [52]).

Appendix D: Computation of the Support for the $\beta = 2$ Dyson's Brownian Motion

We consider the Dyson's Brownian motion with $\beta = 2$ where the positions $\lambda_i(t)$ of N particles evolve in time via Eq. (5), starting from the initial positions $\vec{a}$ at $t = 0$. One defines the Green's function $G_N(z,t)$

$$G_N(z;t) = \frac{1}{N} \sum_{i=1}^{N} \frac{1}{z - \lambda_i(t)}. \quad \text{(D1)}$$

The average density can be obtained via the Sochocki–Plemelj formula

$$\rho(\lambda; t) = \frac{1}{\pi} \operatorname{Im} G_N(z - i0^+; t) \ . \tag{D2}$$

In the large N limit, this converges to

$$G(z; t) = G_\infty(z, t) = \int \frac{\rho(\lambda; t)}{z - \lambda} d\lambda \ , \tag{D3}$$

where $\rho(\lambda; t)$ is the average density at time t. Thus the initial condition for $G(z; t)$ reads

$$G(z; t = 0) = G_0(z) = \int \frac{\rho(\lambda; 0)}{z - \lambda} d\lambda \ , \tag{D4}$$

where $\rho(\lambda; 0)$ is the initial density. In the large N limit, one can show that $G(z, t)$ satisfies the inviscid Burgers' equation [38–41]

$$\partial_t G(t) + G(z, t)\partial_z G(z, t) = 0 \ . \tag{D5}$$

The solution can be obtained in the parametric form by the method of characteristics, as discussed in Sect. 3. It reads

$$G(z; t) = G_0(\xi) \ , \tag{D6}$$

where ξ and z are related by

$$z = \xi + t\, G_0(\xi) \ . \tag{D7}$$

Given z and t, we need to solve Eq. (D7) for ξ and then substitute in Eq. (D6) to obtain $G(z; t)$.

Let us first discuss some general properties of the Green's function $G(z; t)$. Consider first $G(z; t)$ as a function of z along the positive real axis. An exactly similar analysis can be done on the negative real axis. From the definition in Eq. (D1), it is clear that as $z \to \infty$, $G(z; t) \simeq 1/z$ since $\rho(\lambda; t)$ is normalized to 1. As z decreases from $+\infty$, $G(z; t)$ typically increases with decreasing z. However, this does not go on for ever since we expect that there will be a cut along the real axis where $G(z; t)$ acquires a nonzero imaginary part, which gives rise to a nonzero density via Eq. (D2). Let $z_{\text{edge}}(t)$ denote this value of z below which $G(z; t)$ is imaginary. Clearly, this is also the *upper edge* of the support of the density. Thus in the range $[z_{\text{edge}}(t), +\infty)$, $G(z; t)$ is a monotonically decreasing function of z. Similarly, the function $G_0(\xi)$ is, generically, a monotonically decreasing function of ξ for $\xi \in [\xi_{\text{edge}}, +\infty)$ and decays for large ξ as $G_0(\xi) \simeq 1/\xi$. Note that, for simplicity, we have presented only the behavior for the upper edge of the support of the density. A similar analysis can be done for the lower edge of the support, for which we need to analyse the Green's function $G(z; t)$ on the negative real axis in the complex z-plane.

Given z and t, we now want to find the solution for ξ from Eq. (D7). Suppose that we plot z as a function of ξ for $\xi > \xi_{\text{edge}}$. The rhs of (D7) is the sum of two terms: the first one increases linearly with ξ while the second term, for fixed t, is a decreasing function of ξ. Hence their sum, when plotted as a function of ξ will first decrease with increasing ξ, achieves a minimum at $\xi_c(t)$ and then increases monotonically with ξ (see Fig. 9). For a given z and t, this equation (D7) has typically two solutions $\xi_1(z) < \xi_2(z)$. Here, $\xi_2(z)$ is a monotonically increasing function of z, while $\xi_1(z)$ is a monotonically decreasing function of z (see Fig. 9). The correct solution is actually given by $\xi_2(z)$. This is because from Eq. (D6) we see that since $G(z; t)$ is a monotonically decreasing function of z and $G_0(\xi)$ is also a monotonically decreasing function of ξ, hence z must be a monotonically increasing function

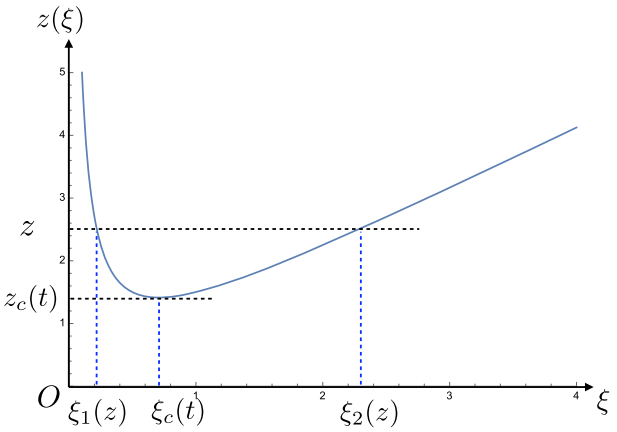

Fig. 9 Plot of $z(\xi)$ in Eq. (D7) for $G_0(\xi) = 1/\xi$ and $t = 1/2$

of ξ. This justifies the fact that $\xi_2(z)$ is the correct root. Note however that $\xi_2(z)$ exists only if $z \geq z_c(t)$ where $z_c(t)$ is the value of $z(\xi) = \xi + t\, G_0(\xi)$ at the minimum located at $\xi = \xi_c(t)$ (see Fig. 9). This minimum is obtained by setting

$$\frac{dz}{d\xi} = 1 + t\, G_0'(\xi) = 0 \,. \tag{D8}$$

This gives the value $\xi_c(t)$ and consequently

$$z_c(t) = \xi_c(t) + t\, G_0(\xi_c(t)) \,. \tag{D9}$$

Therefore we see that the real solution exists only for $z \geq z_c(t)$. Thus we identify

$$z_{\text{edge}}(t) = z_c(t) \,. \tag{D10}$$

As an example, let us consider the simple case where all the particles start at the origin, i.e. $\rho(\lambda; 0) = \delta(\lambda)$. In this case, from Eq. (D4) we have $G_0(\xi) = 1/\xi$. In this case $\xi_{\text{edge}} = 0$. Consequently, from Eq. (D8), we get

$$\xi_c(t) = \sqrt{t} \,. \tag{D11}$$

Note that $\xi_c(t)$ has nothing to do with ξ_{edge}. Here we are considering the positive side of the support, hence we choose the positive root in (D11). Similarly, when analyzing the lower edge of the support, we should instead choose the negative root $\xi_c(t) = -\sqrt{t}$. From Eq. (D9) one gets for the positive side

$$z_c(t) = \sqrt{4\,t} \,. \tag{D12}$$

This result tells us how the upper support of the average density evolves with time t. Indeed, in this case, one can solve for ξ from the quadratic equation $z = \xi + t/\xi$, which gives two roots: $\xi_1(z) = (z - \sqrt{z^2 - 4})/2$ and $\xi_2(z) = (z + \sqrt{z^2 - 4t})/2$. As argued earlier, we choose the second branch as the correct one, i.e., $\xi = (z + \sqrt{z^2 - 4t})/2$. Consequently, from Eq. (D6) one gets

$$G(z; t) = G_0(\xi) = \frac{2}{z + \sqrt{z^2 - 4t}} = \frac{1}{2t}\left(z - \sqrt{z^2 - 4t}\right) \,. \tag{D13}$$

Therefore, from the relation (D2), the average density at time t is given by the semi-circular form

$$\rho(\lambda; t) = \frac{1}{2\pi t}\sqrt{4t - \lambda^2}\,. \tag{D14}$$

Hence we see that the density is supported over the interval $[-\sqrt{4t}, +\sqrt{4t}]$ and indeed the upper support $\sqrt{4t}$ coincides with the value of $z_c(t) = z_{\text{edge}}(t)$ in Eqs. (D10) and (D12).

References

1. Doob, J.L.: Conditional Brownian motion and the boundary limits of harmonic functions. Bull. Soc. Math. Fr. **85**, 431 (1957)
2. Fitzsimmons, P., Pitman, J., Yor, M.: Markovian bridges: construction, Palm interpretation, and splicing, In: Seminar on Stochastic Processes, 1992 (Springer, 1993) pp. 101–134
3. Orland, H.: Generating transition paths by Langevin bridges. J. Chem. Phys. **134**, 174114 (2011)
4. Chetrite, R., Touchette, H.: Nonequilibrium microcanonical and canonical ensembles and their equivalence. Phys. Rev. Lett. **111**, 120601 (2013)
5. Majumdar, S.N., Orland, H.: Effective Langevin equations for constrained stochastic processes. J. Stat. Mech. Theor. Exp. **2015**, P06039 (2015)
6. Chetrite, R., Touchette, H.: Nonequilibrium Markov processes conditioned on large deviations. Ann. Henri Poincaré **16**, 2005 (2015)
7. de Gennes, P.G.: Soluble model for fibrous structures with steric constraints. J. Chem. Phys. **48**, 2257 (1968)
8. Fisher, M.E.: Walks, walls, wetting, and melting. J. Stat. Phys. **34**, 667 (1984)
9. Huse, D.A., Fisher, M.E.: Commensurate melting, domain walls, and dislocations. Phys. Rev. B **29**, 239 (1984)
10. Johansson, K.: Non-intersecting paths, random tilings and random matrices. Probab. Theory Rel. **123**, 225 (2002)
11. Prähofer, M., Spohn, H.: Scale invariance of the PNG droplet and the Airy process. J. Stat. Phys. **108**, 1071 (2002)
12. Katori, M., Tanemura, H.: Symmetry of matrix-valued stochastic processes and noncolliding diffusion particle systems. J. Math. Phys. **45**, 3058 (2004)
13. Tracy, C.A., Widom, H.: Nonintersecting brownian excursions. Ann. Appl. Probab. **17**, 953 (2007)
14. Schehr, G., Majumdar, S.N., Comtet, A., Randon-Furling, J.: Exact distribution of the maximal height of p vicious walkers. Phys. Rev. Lett. **101**, 150601 (2008a)
15. Borodin, A., Ferrari, P., Prahofer, M., Sasamoto, T., Warren, J.: Maximum of Dyson Brownian motion and non-colliding systems with a boundary. Electron. Commun. Prob. **14**, 486 (2009)
16. Nadal, C., Majumdar, S.N.: Nonintersecting Brownian interfaces and Wishart random matrices. Phys. Rev. E **79**, 061117 (2009)
17. Rambeau, J., Schehr, G.: Extremal statistics of curved growing interfaces in 1+ 1 dimensions. EPL **91**, 60006 (2010)
18. Forrester, P.J., Majumdar, S.N., Schehr, G.: Non-intersecting Brownian walkers and Yang-Mills theory on the sphere. Nucl. Phys. B **844**, 500 (2011)
19. Schehr, G., Majumdar, S.N., Comtet, A., Forrester, P.J.: Reunion probability of N vicious walkers: typical and large fluctuations for large N. J. Stat. Phys. **150**, 491 (2013)
20. Nguyen, G.B., Remenik, D.: Extreme statistics of non-intersecting Brownian paths. Electron. J. Probab. **22**, (2017)
21. Le Doussal, P., Majumdar, S.N., Schehr, G.: Periodic Airy process and equilibrium dynamics of edge fermions in a trap. Ann. Phys. **383**, 312 (2017)
22. Gautié, T., Le Doussal, P., Majumdar, S.N., Schehr, G.: Non-crossing Brownian paths and Dyson Brownian motion under a moving boundary. J. Stat. Phys. **177**, 752 (2019)
23. Krattenthaler, C., Guttmann, A.J., Viennot, X.G.: Vicious walkers, friendly walkers and Young tableaux: II. With a wall. J. Phys. A **33**, 8835 (2000)
24. Bonichon, N., Mosbah, M.: Watermelon uniform random generation with applications. Theor. Comput. Sci. **307**, 241 (2003)
25. Marino, M.: Chern–Simons theory, matrix integrals, and perturbative three-manifold invariants. Commun. Math. Phys. **253**, 25 (2005)

26. Mariño, M.: Matrix Models and Topological Strings, In: Applications of Random Matrices in Physics, edited by É. Brézin, V. Kazakov, D. Serban, P. Wiegmann, and A. Zabrodin (Springer Netherlands, Dordrecht, 2006) pp. 319–378
27. Dolivet, Y., Tierz, M.: Chern–Simons matrix models and Stieltjes–Wigert polynomials. J. Math. Phys. **48**, 023507 (2007)
28. Szabo, R.J., Tierz, M.: Chern–Simons matrix models, two-dimensional Yang–Mills theory and the Sutherland model. J. Phys. A **43**, 265401 (2010)
29. Takahashi, Y., Katori, M.: Noncolliding Brownian motion with drift and time-dependent Stieltjes–Wigert determinantal point process. J. Math. Phys. **53**, 103305 (2012)
30. Borot, G., Guionnet, A., Kozlowski, K.K.: Asymptotic expansion of a partition function related to the sinh-model, arXiv: 1412.7721 (Springer, 2016)
31. Guionnet, A.: First order asymptotics of matrix integrals; a rigorous approach towards the understanding of matrix models. Commun. Math. Phys. **244**, 527 (2004)
32. Bun, J., Bouchaud, J.-P., Majumdar, S.N., Potters, M.: Instanton approach to large N Harish–Chandra–Itzykson–Zuber Integrals. Phys. Rev. Lett. **113**, 070201 (2014)
33. Menon, G.: The complex Burgers' equation, the HCIZ integral and the Calogero-Moser system, preprint (2017)
34. Dyson, F.J.: A brownian motion model for the eigenvalues of a random matrix. J. Math. Phys. **3**, 1191 (1962)
35. Dumitriu, I., Edelman, A.: Matrix models for beta ensembles. J. Math. Phys. **43**, 5830 (2002)
36. Rambeau, J., Schehr, G.: Distribution of the time at which N vicious walkers reach their maximal height. Phys. Rev. E **83**, 061146 (2011)
37. Karlin, S., McGregor, J.: Coincidence properties of birth and death processes. Pacific J. Math. **9**, 1109 (1959)
38. Blaizot, J.-P., Nowak, M.A.: Coincidence properties of birth and death processes. Phys. Rev. E **82**, 051115 (2010)
39. Allez, R., Bouchaud, J.-P., Guionnet, A.: Invariant beta ensembles and the Gauss–Wigner crossover. Phys. Rev. Lett. **109**, 094102 (2012)
40. Blaizot, J.-P., Grela, J., Nowak, M.A., Warchoł, P.: Diffusion in the space of complex hermitian matrices. Acta Phys. Pol. B **46**, 1801 (2015)
41. Krajenbrink, A., Doussal, P.L., O'Connell, N.: Tilted elastic lines with columnar and point disorder, non-Hermitian quantum mechanics and spiked random matrices: pinning and localization, preprint arXiv:2009.11284 (2020)
42. Forrester, P.J.: Global and local scaling limits for the $\beta = 2$ Stieltjes–Wigert random matrix ensemble, arXiv preprint arXiv:2011.11783 (2020)
43. Wikipedia, "Cubic equation", https://en.wikipedia.org/w/index.php?title=Cubic_equation&oldid=1005257159 (2021a)
44. Wikipedia, "Quartic function", https://en.wikipedia.org/w/index.php?title=Quartic_function&oldid=1004178910 (2021b)
45. Forrester, P.J., Grela, J.: Hydrodynamical spectral evolution for random matrices. J. Phys. A **49**, 085203 (2016)
46. Borodin, A.: Biorthogonal ensembles. Nucl. Phys. B **536**, 704 (1998)
47. Muttalib, K.A.: Random matrix models with additional interactions. J. Phys. A **28**, L159 (1995)
48. Borodin, A., Strahov, E.: Averages of characteristic polynomials in random matrix theory. Commun. Pure Appl. Math. **59**, 161 (2006)
49. Forrester, P.J., Liu, D.-Z.: Singular values for products of complex Ginibre Matrices with a source: hard edge limit and phase transition. Commun. Math. Phys. **344**, 333 (2016)
50. Fyodorov, Y.V., Grela, J., Strahov, E.: On characteristic polynomials for a generalized chiral random matrix ensemble with a source. J. Phys. A **51**, 134003 (2018)
51. Grela, J., Nowak, M.A., Tarnowski, W.: Eikonal formulation of large dynamical random matrix models, preprint, arXiv:2010.01690 (2020)
52. Szmytkowski, R.: On the derivatives $\partial^2 P_\nu(z)/\partial^2\nu$ and $\partial Q_\nu(z)/\partial\nu$ of the Legendre functions with respect to their degrees. Integr. Transf. Spec. Fr. **28**, 645 (2017)